Formation and Circulation Processes of Intermediate Water in the Japan Sea

YUTAKA YOSHIKAWA, TOSHIYUKI AWAJI, AND KAZUNORI AKITOMO

Department of Geophysics, Kyoto University, Kyoto, Japan

(Manuscript received 14 July 1997, in final form 23 July 1998)

ABSTRACT

The formation and circulation processes of intermediate water in the Japan Sea have been investigated by study of the subduction of mixed layer water. To simulate realistic seasonal variations in the velocity and hydrographic structures, a numerical model with a nudging method for potential temperature and salinity, which reproduced the general features in the Japan Sea, is used. Close investigation of the subduction process reveals two major formation areas (A and B) of intermediate water. Area A (41°~43°N, west of 135°E) corresponds to the region reported by recent observations, whereas Area B (40°~43°N, east of 136°E) has not been reported so far. The mixed layer water subducted in Area A is advected southwestward and eventually its upper portion (above 200 m) reaches the eastern part of the Japan Basin, whereas the lower branch (below 200 m) reaches the Tsushima Basin. This indicates that the East Sea Intermediate Water originates from the mixed layer in Area A, and suggests that the East Sea Intermediate Water and the upper portion of the Japan Sea Proper Water represent the same type of intermediate water. In contrast, the water subducted in Area B is advected northward and some of it flows out through the Soya Strait, while another portion is reentrained into the mixed layer off the Primorye coast. Tracking of the subducted water particles clearly shows that the southward transport of the intermediate water takes a seasonally varying path: for example, a path along the continental coast in winter and one along the Japanese coast in summer. The total formation rate of the intermediate water is estimated to range between 0.48 and 0.69 ($\times 10^6$ m^3 s^{-1}) according to the strength of nudging terms, and the corresponding range in ventilation time is 20.3~25.6 years.

1. Introduction

The Japan Sea is a marginal sea of the northwest midlatitude Pacific. It is enclosed by the Eurasian continent and the Japanese Islands and connects with the North Pacific through the Tsushima and Tsugaru Straits and with the Okhotsk Sea through the Soya and Mamiya Straits (Fig. 1). It contains three major basins called the Japan, Tsushima, and Yamato Basins, and a high central seamount called the Yamato Rise (YR).

The circulation in the Japan Sea (schematically shown in Fig. 2) is thought to be driven by the net pressure difference between the south and north straits (e.g., Minato and Kimura 1980; Ohshima 1994), wind stress, and thermohaline forcing (e.g., Seung and Kim 1989). Through the Tsushima Strait, the warm and saline Pacific water (Tsushima Warm Water) advects into the surface layer (above 300 m) of the southern Japan Sea (Warm Current Region; Moriyasu 1972) as the Tsushima Warm Current driven by the net pressure difference mentioned above. The behavior of this current has been well documented in previous studies (e.g., Moriyasu 1972; Yoon 1982; Katoh 1994). After passing through the Tsushima Strait, it bifurcates into two distinct branches—an eastern flow called the Nearshore Branch (NB) flowing northward along the Japanese coast as a density current and a western component called the East Korean Warm Current (EKWC), which is the western boundary current along the Korean coast. The EKWC separates from the coast where it meets the southward flowing Liman Cold Current (LCC) or the North Korean Cold Current (NKCC), and both currents turn eastward to flow roughly along 40°N latitude, forming the subpolar front between the Tsushima Warm Water (TWW) and the cold and fresh water to the north. This TWW is also separated from the underlying cold and fresh deep water by the pycnocline. To the north of the subpolar front, a cyclonic subpolar gyre exists comprising the southward LCC/NKCC, the eastward current along the subpolar front, and the northward flow off Hokkaido. This subpolar region was called the ''Cold Current Region'' by Moriyasu (1972). The dynamics of the surface current system described above have been elucidated, primarily through numerical studies initiated by Yoon (1982).

It is worth mentioning that Kitani (1987) estimated the volume of the TWW to be 8×10^4 km^3, which occupies only 5% of the total volume of the Japan Sea. This fact means that the remaining 95% is below the

Corresponding author address: Dr. Yutaka Yoshikawa, Department of Geophysics, Kyoto University, Kyoto 606-8502, Japan.
E-mail: yosikawa@kugi.kyoto-u.ac.jp

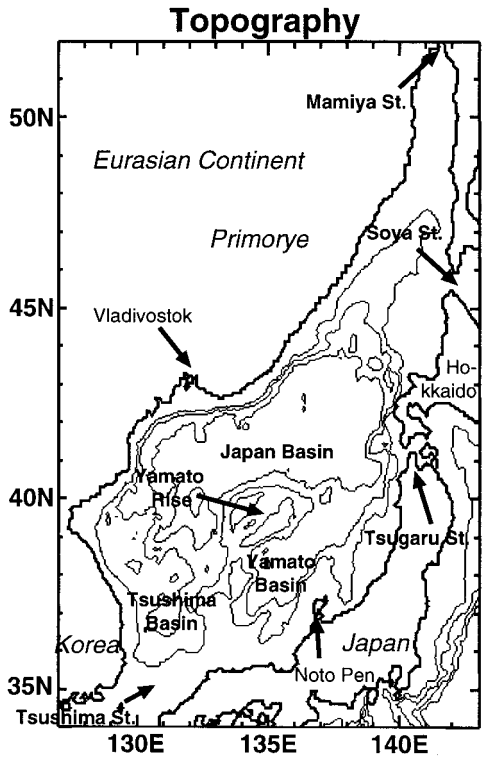

FIG. 1. Topography of the Japan Sea. Contour intervals are spaced at 1000 m.

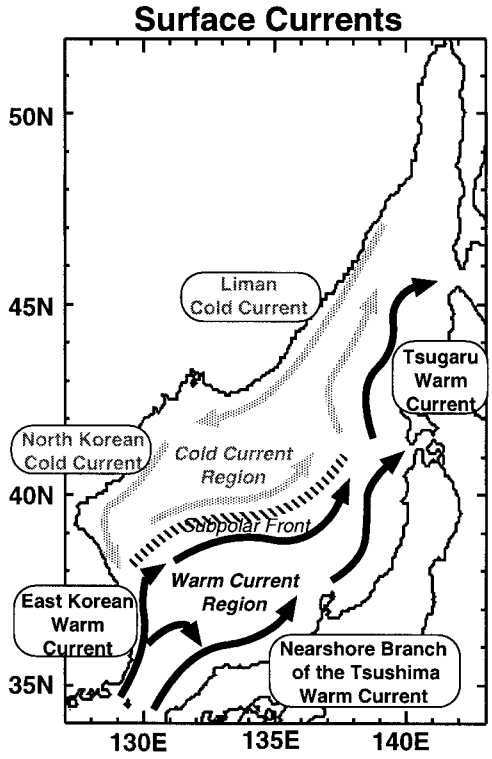

FIG. 2. Schematic picture of surface current structures (after Uda 1934). Black arrows indicate warm currents, and gray ones indicate cold currents.

pycnocline and thus deep-water formation and related circulation processes are subjects of great importance in our understanding of the heat and material transports in the Japan Sea.

The deep water of the Japan Sea is believed to be formed by local winter convection since all the straits connecting the Japan Sea to the neighboring oceans (the North Pacific and the Okhotsk Sea) are so shallow ($\leq$200 m) that they prevent direct exchange of the deep waters. In fact, the deep water has lower salinity and higher dissolved oxygen than other deep waters. For this reason, Uda (1934) called it the ''Japan Sea Proper Water'' (JSPW). This JSPW has been long recognized as a single water mass because of its general homogeneity ($0^{\circ}\text{C} < \theta < 1^{\circ}\text{C}$, 33.96 psu $< S <$ 34.14 psu) (e.g., Yasui et al. 1967). However, Nitani (1972) found the presence of two different vertical gradients of potential temperature in deep layers from measurements in 1969 and 1971, and classified the JSPW into three components—the Japan Sea Deep Water (~1000 m), the Upper Bottom Water (1000 m~2000 m), and the Lower Bottom Water (~2000 m). He suggested that the source region of the Japan Sea Deep Water should lie off the Primorye coast. Although his analysis provided the first insight into the deep-water mass structure and region of generation, some uncertainties remain in his determination because of the use of a short two-year dataset for the definition of each physical quantity. Taking this point into consideration, Sudo (1986) made a rather comprehensive water mass analysis using all available data for salinity, potential density, and dissolved oxygen along with potential temperature. Consequently, the distinct discontinuity centered at about 700-m depth was found in both vertical profiles of salinity and dissolved oxygen, facilitating a more reasonable classification of the deep waters below the pycnocline into two water masses—the upper portion of the JSPW (UJSPW), characterized by low salinity and high dissolved oxygen, and the deeper water.

In order to characterize the general features of the UJSPW, Senjyu and Sudo (1993, 1994) made climatological maps for several water properties on each isopycnal surface and revealed that the UJSPW ranges between 32.00 and 32.05 σ_1. Further, they confirmed that, as judged from the Redfield ratio of oxygen consumption to phosphate regeneration (Redfield et al. 1963), it has a single source in the area of 40°~43°N, west of 136°E. This result is similar to that obtained in a recent analysis by Seung and Yoon (1995a), using historical Russian hydrographic data, and shows the occurrence of significant deep convection in wintertime. (In fact, this takes place in a narrow region between fresh surface water along the continental coast and warm offshore water in the Warm Current Region.)

Based on wintertime climatological maps of potential vorticity and dissolved oxygen concentration, Senjyu

and Sudo (1993, 1994) suggested the following transport process for the UJSPW: The newly formed UJSPW moves southwestward along the continental coast through the effect of earth rotation and arrives at the region west of the YR. Later, a large portion turns eastward and finally enters the Yamato Basin via the north or south of the YR. The formation rate of the UJSPW was roughly estimated to be about 1.5×10^4 km^3 yr^{-1} ($=0.48$ Sv) (Sv $\equiv 10^6$ m^3 s^{-1}) from the volume of the outcropping water. The advection timescale from the formation region to the Yamato Basin was inferred to be 12~15 months (Senjyu and Sudo 1996). These results gave a basic description of the UJSPW. In the Japan Sea, however, seasonal variations in the velocity field are so strong from surface to bottom (Seung and Yoon 1995b) that an understanding of their effect on the transport processes is required.

Another important feature observed below pycnocline in the Japan Sea is the presence of intermediate water in the Tsushima Basin [called the East Sea (Japan Sea) Intermediate Water (ESIW)], characterized by a salinity minimum and dissolved oxygen maximum centered at about 200 m (Kim and Chung 1984). However, the formation mechanism of the ESIW and its location, the relation between the UJSPW and the ESIW, and the processes responsible for the deep transport are still unclear. To understand these, an investigation is needed to clarify the detailed sources and pathways of deep water masses, particularly in these two waters, in relation to the seasonal variations in the velocity and hydrographic fields.

One useful approach to accomplish this aim is the use of ocean general circulation models (OGCMs), and hence several numerical simulations have been made to date focusing on the dynamics of the Japan Sea circulation. In particular, Seung and Kim (1993) modeled not only the surface but also the deep circulation in the Japan Sea using a prognostic model with realistic bottom topography and succeeded in reproducing some typical circulation features. However, problems remained in their results: they observed an overshooting of the modeled EKWC and their deep layer was warmer than the observational results. Holloway et al. (1995) showed that the unrealistic overshooting of the EKWC can be greatly improved by including mean flow forcing due to an eddy–topography interaction called ''topostress'' into the numerical model. Though their study advanced our knowledge of some modeled circulation features in the Japan Sea, it was directed rather to circulation dynamics. In addition, systematic errors remained, for example, in reproducing vertical distributions of potential temperature and salinity of interest to us, leading to excess temperature and low salinity at middepth, which in turn lead to a prediction of northward flow beneath the NB [which is inconsistent with recent observations (southward) by Hase et al. (1997)]. Their problems most likely stem from poor knowledge of the eddy parameter. To improve these deficiencies, Seung and Yoon (1995b) used a robust diagnostic model with the so-called γ terms (or nudging terms) (Sarmiento and Bryan 1982) to restore the potential temperature and salinity to the observed values. In this case, the overshooting of the EKWC was much reduced and the simulated velocity field was similar to that of the observations. Unfortunately, any investigation using the robust diagnostic models requires a time series of observed potential temperature and salinity for all grids over the study period (Sarmiento and Bryan 1982; Miyama et al. 1995). It was the lack of such a full dataset covering the entire Japan Sea (particularly the deep layer as shown later) and for all seasons that limited their study to the steady model for specified seasons. Thus our understanding of the seasonally varying processes of the velocity and hydrographic fields, which are particularly important when considering deep water formation processes (e.g., Williams et al. 1995), is still limited.

In this study, in order to reproduce the full seasonal cycle of the Japan Sea circulation using the existing hydrographic data, we incorporate a ''nudging method'' for potential temperature and salinity into the OGCM, as with the conventional robust diagnostic model, but only for grids containing observations throughout a year. This numerical approach is a particularly attractive data assimilation technique for oceanographic scenarios with low-density observations in both space and time, as compared with, for example, meteorology (Ghil and Malanotte-Rizzoli 1991; Haines et al. 1993).

After investigation of the seasonal behavior of the calculated velocity and hydrographic fields, we track the Lagrangian movement of water particles subducted from the mixed layer into the deep layer using the Euler–Lagrangian technique (Awaji 1982; Miyama et al. 1995) in order to further our understanding of the deep water formation and its circulation processes in the Japan Sea. In doing so, quite poor observational and theoretical knowledge of the deeper layer structure to date (Senjyu and Sudo 1994; Seung and Yoon 1995a) directed our attention primarily to behavior within both the UJSPW and the ESIW as described earlier. Taking into consideration previous observational results, for convenience, we classify the Japan Sea deep waters into two water masses: ''the intermediate water'' above about 700-m~1000-m depth, characterized by low salinity and high dissolved oxygen and ''the deeper water'' below. Thus the intermediate water defined here involves both the UJSPW and the ESIW. We attempt to analyze the detailed subduction processes of this intermediate water and then briefly consider the deeper water. This approach contributes to a better understanding of deep ventilation in the open oceans because the Japan Sea has many similarities with open ocean situations, even though it is a marginal sea, and hence it can be viewed as a natural laboratory (Holloway et al. 1995). In addition, the Japan Sea has the advantage of small area (about 150 times smaller than the Pacific) and this makes our task of simulating the deep ventilation processes

TABLE 1. Thickness of model levels.

Depth range (m)	Level thickness (m)	Number of levels
0m ~ 100m	20m	5
100m ~ 400m	50m	6
400m ~ 600m	100m	2
600m ~ 1000m	200m	2
1000m ~	500m	5

easier due to its small size. This benefits collaboration between observers and modelers.

This paper is organized as follows. In section 2 both the method of constructing a monthly mean climatology of potential temperature and salinity and the numerical model are described. The features of the seasonal cycle of the modeled velocity and hydrographic fields are given in section 3. The Lagrangian view of the formation and circulation processes of the intermediate water is explained in section 4 and results are discussed in section 5 and summarized in section 6.

2. Formulation of the model

a. Monthly mean climatology of potential temperature and salinity

A nudging approach requires the monthly mean climatology of observed potential temperature (θ*) and salinity (S*) on a numerical grid (described later) whose horizontal resolution is ¼° and whose vertical resolution is as listed in Table 1 (20 levels). First, we simply describe the method of constructing these hydrographic data from the National Oceanic Data Center (NODC) dataset, which comprises approximately 42 000 pairs of θ* and S* in the Japan Sea. After removal of spurious outliers from the range between −2° and 30°C for potential temperature (θ) and 25 and 35 psu for salinity (S), the remaining hydrographic data were interpolated vertically at each station and then averaged onto a common grid. We grouped these gridded data into four seasons: winter (Jan–Mar), spring (Apr–Jun), summer (Jul–Sep), autumn (Oct–Dec), and further into two subregions (north and south of 40°N). For each subgroup, a mean curve of θ versus S (i.e., θ–S diagram) was determined and standard deviation values from this mean curve were then calculated. All data outside the two-standard-deviation boundaries were rejected for quality control.

At the top level, observed data covering all grids throughout a year must give thermohaline forcing at the sea surface in the manner of Haney (1971) (i.e., Newtonian damping of θ and S to observed values). This was performed using an objective analysis scheme introduced by Levitus (1982). A first guess field was determined by the same method as in Levitus (1982) with the exception that in winter it was done subjectively in reference to climatological hydrographic maps of the Japan Oceanographic Data Center (JODC) (1978), to avoid a rather unrealistic analysis field due to the shortage of observations. Finally, the gridded data for each season were interpolated to give monthly θ* and S* values using the cubic spline fit (Armi and Bray 1982).

Figure 3 shows the locations of the grid boxes with obtained θ* and S* at the example depth of 275 m and ratios of the number of these grid boxes to the total grid number at each level. It is obvious that observations to date are very sparse in the Cold Current Region and in the middle and deep layers. The nudging effect therefore works mainly in the Warm Current Region above the pycnocline. This is far from the coverage available in the complete robust diagnostic model. In Fig. 4, maps of the sea surface potential temperature and salinity obtained by the objective scheme described above are shown. Naturally, these pictures are similar to the corresponding climatological maps of the JODC (not shown). However, the latter maps also have uncertainties in the Cold Current Region and hence the distribution of calculated sea surface potential temperature and salinity are less reliable there. The influence this has on our simulation results will be discussed in the next section.

b. Numerical model

The model region covers the entire Japan Sea basin. The geometry of the Japan Sea has been resolved with DBDB5 topographic data (the National Geophysical Data Center, Boulder, Colorado). As mentioned earlier, the horizontal resolution is ¼° × ¼° and vertically there are 20 levels expanding in thickness from 20 m for surface layers to 500 m for deep layers (Table 1).

Under the rigid-lid, Boussinesq, and hydrostatic approximations, the governing equations in spherical coordinates are

$$\frac{\partial u}{\partial t} + L(u) - \frac{uv\tan\phi}{a} - fv = \frac{-1}{\rho_0 a\cos\phi}\frac{\partial p}{\partial \lambda} + F^u, \quad (1)$$

$$\frac{\partial v}{\partial t} + L(v) + \frac{u^2\tan\phi}{a} + fu = \frac{-1}{\rho_0 a}\frac{\partial p}{\partial \phi} + F^v, \quad (2)$$

$$\frac{\partial p}{\partial z} = -\rho g, \quad (3)$$

$$L(1) = 0, \quad (4)$$

$$\frac{\partial \theta}{\partial t} + L(\theta) = \gamma(\theta^* - \theta) + F^\theta, \quad (5)$$

$$\frac{\partial S}{\partial t} + L(S) = \gamma(S^* - S) + F^S, \quad (6)$$

$$\rho = \rho(\theta, S, p), \quad (7)$$

with t time, ϕ latitude, λ longitude, a the radius of the earth (6380 km), g the gravitational acceleration (9.8 m s^{-2}), f ($=2\Omega\sin\phi$) the Coriolis parameter (Ω the angular velocity of the earth), p pressure, ρ_0 the reference

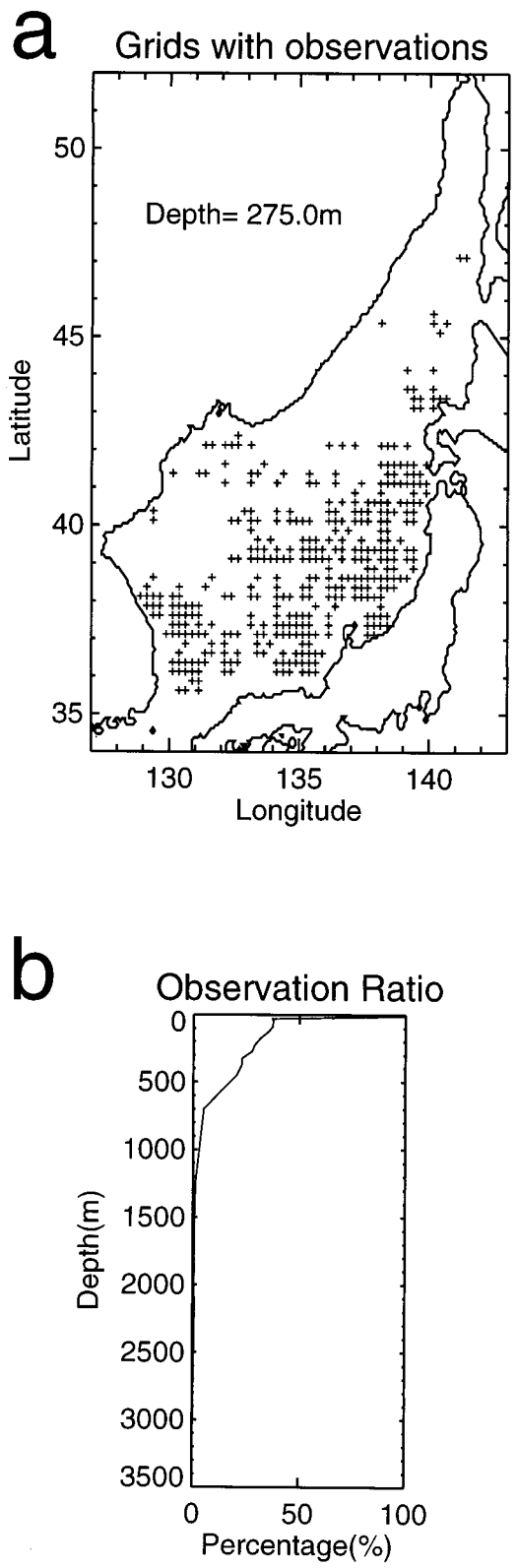

FIG. 3. (a) Distribution of grid boxes (represented by plus signs) where observed potential temperature (θ^*) and salinity (S^*) are obtained at 275-m depth. (b) The ratio of the grid box where θ^* and S^* are obtained as a function of depth.

density of water, and ρ the deviation from ρ_0; u, v, w are the eastward, northward, and upward velocity components, respectively. Here $L(\sigma)$ represents the advection operator defined as

$$L(\sigma) \equiv \frac{1}{a\cos\phi}\frac{\partial}{\partial\lambda}(u\sigma) + \frac{1}{a\cos\phi}\frac{\partial}{\partial\phi}(\cos\phi v\sigma) + \frac{\partial}{\partial z}(w\sigma). \tag{8}$$

The terms in F represent the effects of turbulent viscosity and diffusivity in the harmonic form as

$$F^u = A_{mv}\frac{\partial^2 u}{\partial z^2} + A_{mh}\left[\nabla^2 u + \frac{(1-\tan^2\phi)u}{a^2} - \frac{2\sin\phi}{a^2\cos^2\phi}\frac{\partial v}{\partial\lambda}\right], \tag{9}$$

$$F^v = A_{mv}\frac{\partial^2 v}{\partial z^2} + A_{mh}\left[\nabla^2 v + \frac{(1-\tan^2\phi)v}{a^2} + \frac{2\sin\phi}{a^2\cos^2\phi}\frac{\partial u}{\partial\lambda}\right], \tag{10}$$

$$F^{\theta(S)} = \left[\left(\frac{A_{tv}}{\delta}\right)\frac{\partial^2\theta(S)}{\partial z^2} + \frac{A_{th}}{a^2}\nabla^2\theta(S)\right], \tag{11}$$

where A_{mh} ($=4.0\times10^2$ m^2 s^{-1}) and A_{mv} ($=1.0\times10^{-4}$ m^2 s^{-1}) are the horizontal and vertical eddy viscosity coefficients and A_{th} ($=2.0\times10^2$ m^2 s^{-1}) and A_{tv} ($=0.1\times10^{-4}$ m^2 s^{-1}) are the horizontal and vertical eddy diffusion coefficients, respectively. In (11), δ is concerned with the convective adjustment process; that is,

$$\delta = \begin{cases} 1 & \text{for neutral and stable stratification} \\ 0 & \text{for unstable stratification.} \end{cases}$$

Thus an unstratified water column is instantaneously mixed, as in previous studies. As for (7), a nine-term polynomial approximated to the International Equation of State 80 (UNESCO 1978) is used according to Bryan and Cox (1972).

The first terms in the right-hand side of (5) and (6) represent the nudging terms for θ and S (Ghil and Malanotte-Rizzoli 1991; Miyama et al. 1995). The value of γ^{-1} in this study is set as

$$\gamma^{-1} = \begin{cases} \infty & \text{where the } \theta^* \text{ and } S^* \text{ are not obtained} \\ 1\text{ yr} & \text{where the } \theta^* \text{ and } S^* \text{ are obtained above 1000 m} \\ 3\text{ yr} & \text{where the } \theta^* \text{ and } S^* \text{ are obtained below 1000 m.} \end{cases}$$

The above γ^{-1} value is taken to be larger than that of a full robust diagnostic model of Seung and Yoon (1995b) in order to suppress numerical instability and distortion of model fields due to significant internal

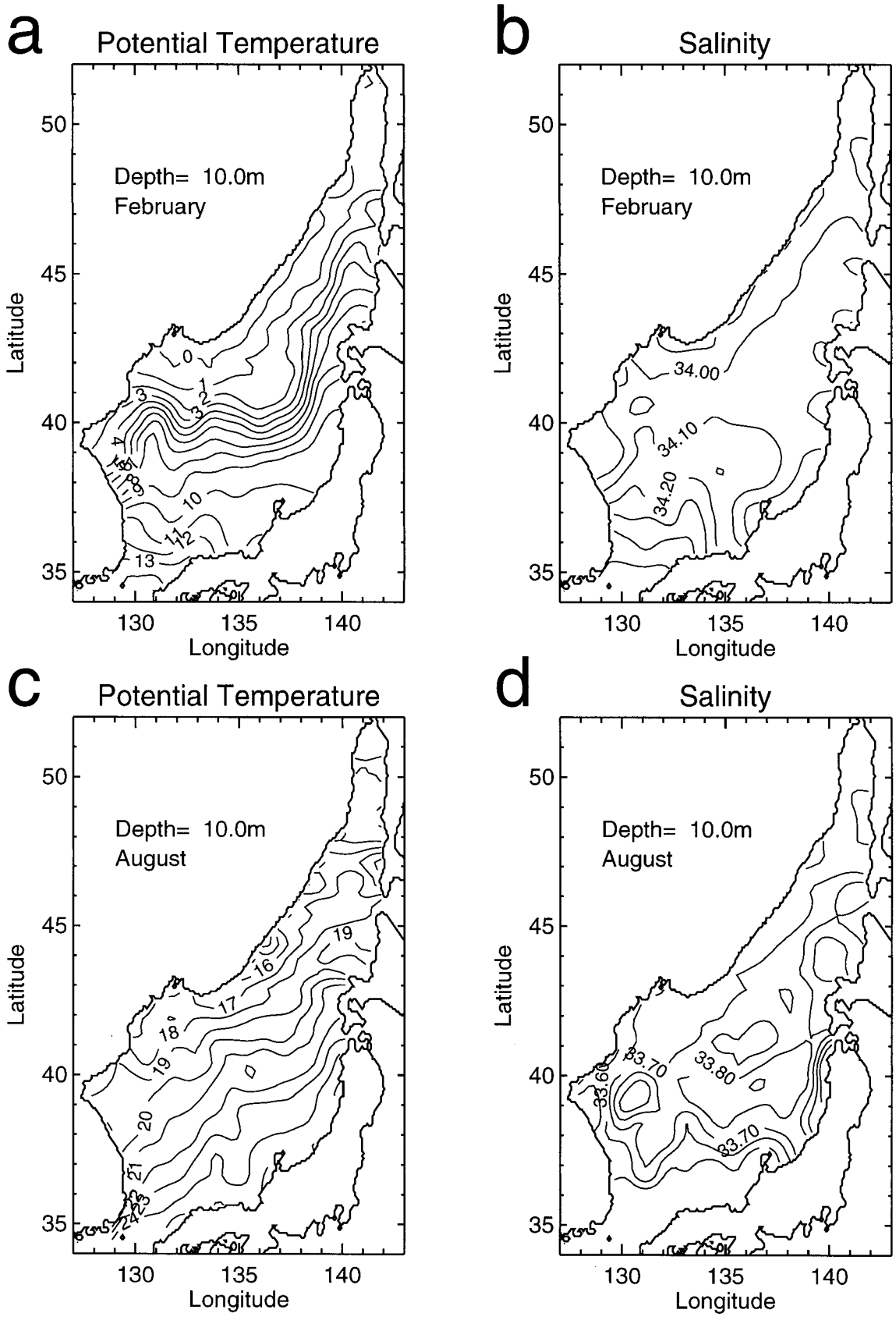
a
Potential Temperature
Depth= 10.0m
February
b
Salinity
Depth= 10.0m
February
34.00
34.10
34.20
c
Potential Temperature
Depth= 10.0m
August
d
Salinity
Depth= 10.0m
August
33.60
33.70
33.80
33.70
Latitude
Longitude
50
45
40
35
130
135
140

sources of θ and S for small γ^{-1} values generated through the nudging terms, especially in regions of sparse distribution of θ^* and S^* (Fig. 3). The sensitivity of our model result to the choice of γ^{-1} will be discussed in section 5.

The boundary conditions are as follows: At the sea surface, a wind stress from the monthly mean climatology of Na et al. (1992) is imposed. Sea surface heat and salt fluxes are given by the Newtonian damping of potential temperature and salinity at the top layer to the monthly climatological values (Haney 1971) with a timescale (γ^{-1}) of 0.5 day. A no-slip condition is imposed at land and bottom boundaries. Inflow through the Tsushima Strait is fixed to be 2.2 Sv and outflow through the Tsugaru and Soya Straits is set at 1.4 Sv and 0.8 Sv, respectively, in accord with recent observations (Katoh 1993; Shikama 1994). At these open boundaries, a baroclinic component of velocity is determined using θ^* and S^* values. In this study, volume transport through Mamiya Strait is neglected due to its smallness ($\sim$0.03 Sv; Aota and Ishikawa 1991).

After spinup for 20 years using the annual mean forcing, a 7-yr integration using the seasonal forcing is made, by which time the model almost reaches an equilibrium seasonal cycle. The results to be shown here are from the last year of the integration.

3. Simulated velocity and hydrographic fields in the Japan Sea

The essential features of the annual cycle of the velocity and hydrographic fields in the Japan Sea can be outlined on the basis of winter and summer data. Figures 5 and 6 illustrate the velocity fields in February and August as representing winter and summer, respectively. In February, due to the large positive wind stress curl and strong surface cooling in the northern half of the Japan Sea, the depth-averaged cyclonic circulation is significant in the Cold Current Region (Fig. 5a), as suggested by Seung and Kim (1989). In the surface layer (10 m; Fig. 5b), the LCC/NKCC flows southwestward along the continental coast and the EKWC separates from the Korean coast at around 37°N. Though the overshooting of the EKWC is suppressed relative to the prognostic models, it still flows farther northward after separation than is observed. One reason for this is that the observed surface potential temperature and salinity used there to derive air–sea fluxes strongly reflect the properties of warm eddies that frequently form off the Korean coast at 40°N (Fig. 4a) (Isoda and Nishihara 1992). Actually the EKWC flows along the periphery of these eddies from the geostrophic relation. Another possible reason relates to the pycnocline depth, which will be discussed in detail in section 5. The NB flowing along the northern coast of Japan is less visible in winter. These results show that typical features of the surface velocity fields in winter are successfully reproduced.

In the intermediate layer (450 m; Fig. 5c), a strong counterclockwise current can be seen flowing along the Primorye coast to the Noto Peninsula by way of the region offshore of Vladivostok. This current seems to be formed both by the western boundary current driven by the large positive wind stress curl (Yoon and Hirose 1995) and by the internal density current associated with strong surface cooling off the Primorye coast in winter (Senjyu and Sudo 1993). A southwestward current near the eastern flank of the YR observed by Kitani (1987) is not reproduced in the model. A likely reason for this is the rough resolution of the YR geometry since this flow is strongly affected by topography (Kitani 1987).

In August, the effect of wind stress in the Japan Sea circulation becomes negligible and hence the prominent cyclonic circulation, which reaches the bottom in the winter season, is much reduced (Fig. 6a). Associated with this weakening, the EKWC separates from the Korean coast at a more northward location near 39°N. In contrast, because of the inflow of more freshwater and surface heating in the summer season, the effect of baroclinicity dominates and consequently the NB becomes strongest (Fig. 6b). In the intermediate layer (Fig. 6c), associated with the strengthened baroclinicity, a fairly intense southwestward undercurrent beneath the NB emerges from the region west of Hokkaido to the Tsushima Basin along the Japanese coast. The presence of this undercurrent is supported by recent observations by CREAMS (Circulation Research of the East Asian Marginal Seas; Hase et al. 1997) and plays an important role in intermediate transport processes as will be described later. The velocity measurement of Lie et al. (1989) during the period from August to November detected a southward mean current flowing in the intermediate layer along the Korean coast. Though they reported its presence in August, it appears from October to March in our model (not shown). The small delay in its appearance is attributable to a warm cyclonic eddy formed off the Korean coast at 38.5°N in August (Fig. 6c), which is accompanied by overshooting of the simulated EKWC and acts to prevent the southward flow along the coast (Holloway et al. 1995).

The simulated hydrographic field is shown in Fig. 7. In Fig. 7a, the zonal distribution of potential density referred to 1000 db (σ_1) along 41.88°N for March is presented [corresponding to Fig. 12 of Senjyu and Sudo (1993)]. The UJSPW, which ranges from 32.00 to 32.05

←

FIG. 4. Distribution of surface (a) potential temperature for Feb, (b) salinity for Feb, (c) potential temperature for Aug, and (d) salinity for Aug, obtained by the objective analysis scheme described by Levitus (1982). Contour intervals are 1°C for potential temperature and 0.1 psu for salinity.

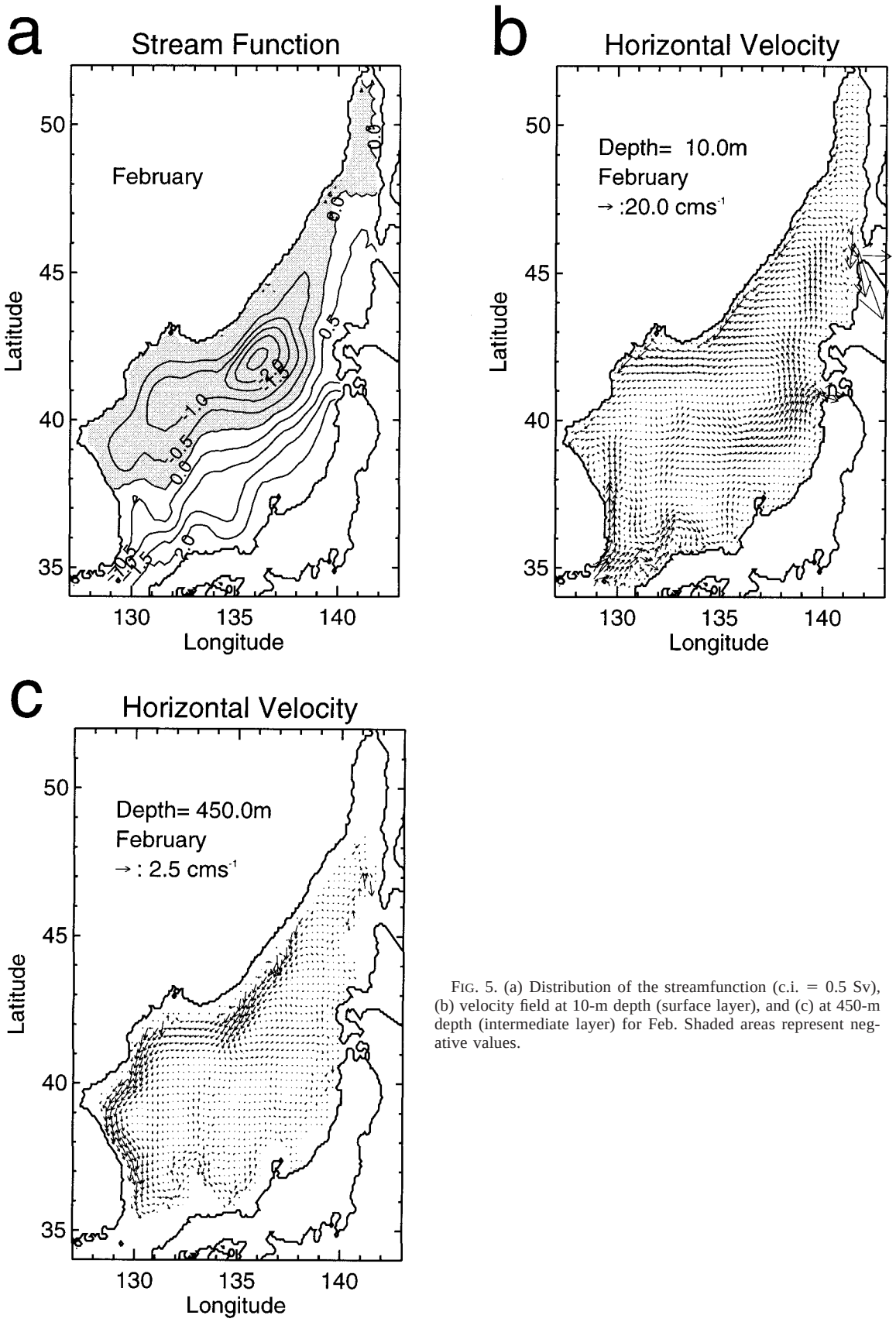

FIG. 5. (a) Distribution of the streamfunction (c.i. = 0.5 Sv), (b) velocity field at 10-m depth (surface layer), and (c) at 450-m depth (intermediate layer) for Feb. Shaded areas represent negative values.

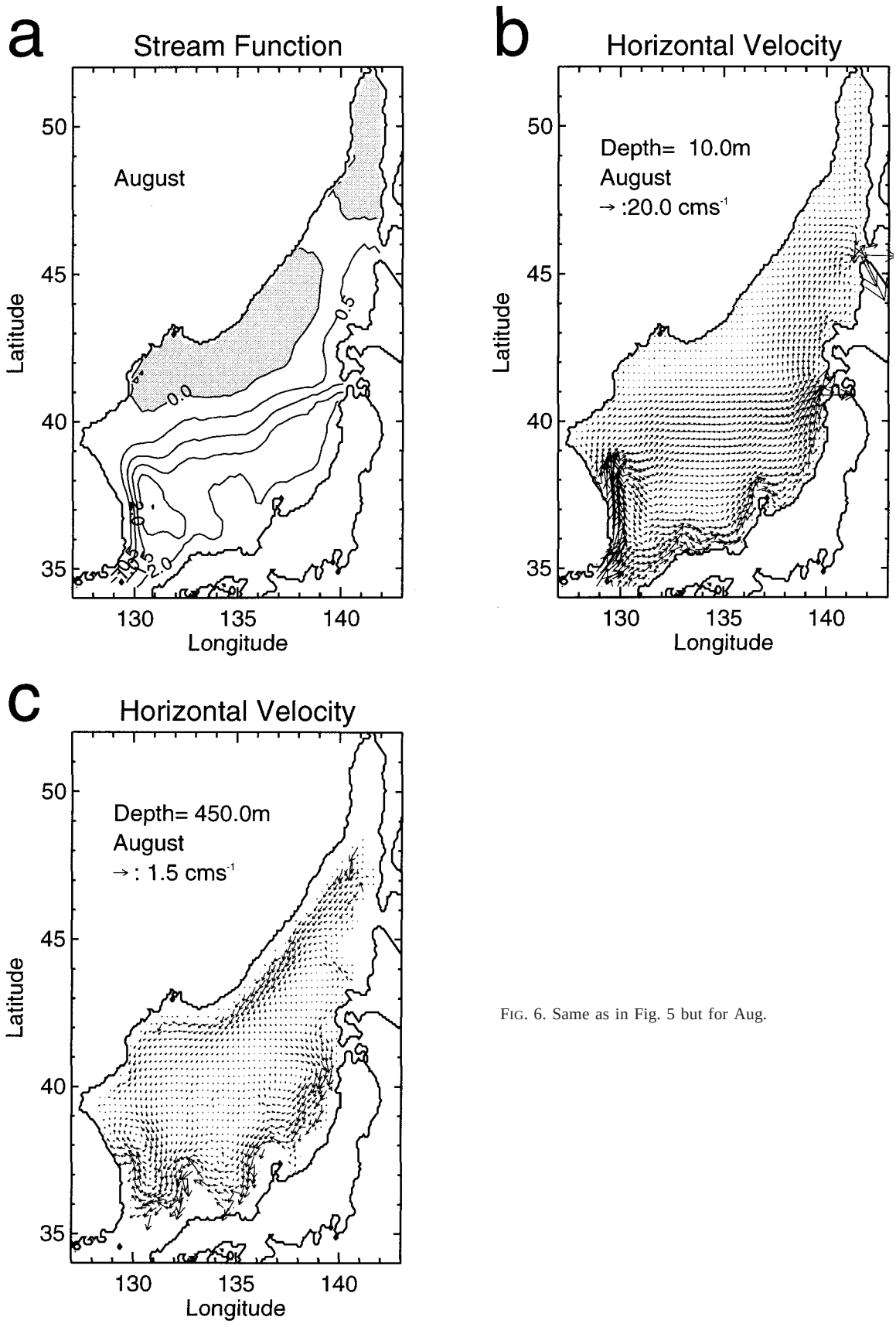

FIG. 6. Same as in Fig. 5 but for Aug.

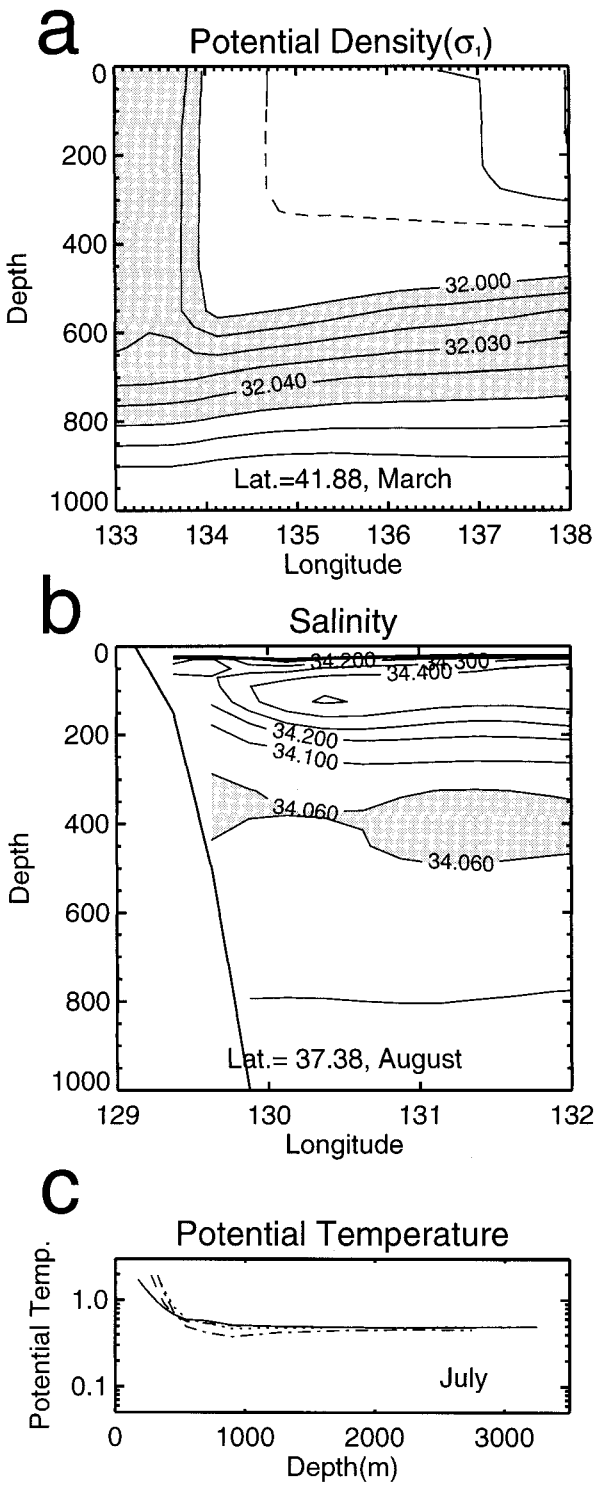

FIG. 7. (a) Zonal distribution of potential density referred to 1000 db at 41.88°N in Mar (c.i. = 0.01 σ_1). The shaded areas denote 32.00 σ_1~32.05 σ_1, corresponding to the UJSPW. (b) Zonal distribution of salinity at 37.38°N in Aug. Areas with salinity lower than 34.06 psu are shaded. (c) Vertical distribution of the average potential temperature in Jul in semilogarithmic coordinates. The solid line is the western part of the Japan Basin, dotted line is the eastern part of the Japan Basin, dashed line is the Tsushima Basin, and dash-dotted line is the Yamato Basin.

σ_1 (shaded areas in Fig. 7a) and is defined by Senjyu and Sudo (1993), is formed by deep convection off the Primorye coast. Though the overall features of the simulated UJSPW are basically similar to the observations, its surface density values are smaller than those observed: simulated convection reaches from the surface down to the 32.02 σ_1 density level, while observations in 1971 showed convection down to the deeper level of 32.05 σ_1. This disagreement may arise from smaller sea surface heat and salt fluxes used in the model than existed in 1971. In fact, the climatological sea surface potential density obtained in section 2a is small compared with that in 1971. Consequently, the calculated sea surface potential density, which is restored to this climatological value with the Haney-type boundary condition, is about 0.03 σ_1 smaller around the formation area of the UJSPW than that in 1971. This small difference corresponds to as much as a 200-m depth difference in the isopycnal surfaces due to the weak stratification.

Figure 7b represents the zonal distribution of salinity along 37.38°N in August. The salinity minimum layer (SML; ≤34.06 psu) can be found between 300- and 400-m depth, while the observed SML water (corresponding to the ESIW) is situated at about 200-m depth (e.g., Kim and Chung 1984). This discrepancy seems to stem from the difference between the simulated and observed pycnocline depths. In our model, since the effect of isopycnal diffusion caused by baroclinic instability (with spatial scales of the Rossby deformation radius ~50 km) is not fully represented due to the insufficient grid resolution of ¼°, downward vertical diffusion of lighter surface water becomes larger than it actually is. Furthermore, the deeper water below 700-m depth is not formed as mentioned below, leading to the weak upwelling of cold deeper water in the southern region. These two factors result in a pycnocline located at a deeper level than is observed.

Basin-averaged vertical profiles of the calculated potential temperature below 200 m in July are shown in Fig. 7c [corresponding to Fig. 1 of Nitani (1972)]. This figure indicates that, though the typical structure above about 600 m is in good agreement with observations, the hydrographic structure below is not well reproduced in the model. For example, the difference between the calculated and observed potential temperature exceeds 0.4°C below 2000 m. The major reason for this can be explained as follows. The deeper water is believed to be formed north of about 43°N (Nitani 1972; Sudo 1986). As described earlier, the magnitude of air–sea heat and salt fluxes in the Haney method are proportional to the difference between the calculated and observed values of potential temperature and salinity. Unfortunately, because of the paucity of hydrographic observations in the northern part of the Japan Sea, the observed values deduced from the Levitus (1982) objective analysis scheme are affected by data in the southern warmer region. This leads to relatively high θ* and

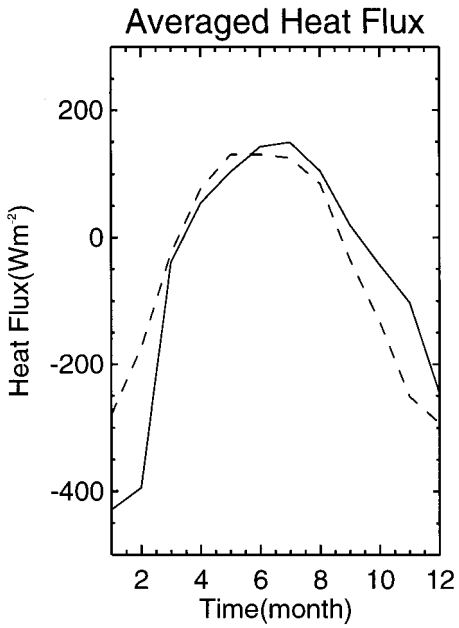

FIG. 8. The monthly mean surface heat flux in the model (solid line) together with Hirose's (1996) heat flux (broken line). Averaged values over the Japan Sea are plotted.

S^* values and consequently smaller air–sea fluxes in the northern part as compared with observation. Thus, convection does not reach great depths in our model. This seems to be inevitable as long as the current climatological dataset of θ^* and S^* in the Japan Sea is used because the heat flux data of Hirose et al. (1996), which were derived from the bulk method using most of the available vessel data, are similar to ours (Fig. 8). In addition to this, it has been recently reported that the deeper water may be formed only in severe winters when heat loss to the atmosphere must be larger than in the climatological winter (Riser 1997). In order to improve this deficiency, much more observations are required, especially in the northern region, and a better parameterization for deep convection is necessary.

Nevertheless, a number of similarities between the simulated velocity field such as the EKWC, LCC/NKCC, and NB and its undercurrent and the observed findings support the notion that our model simulates the basic features of the Japan Sea circulation. In addition, the simulated hydrographic structures of the intermediate water are in good agreement with observations. Therefore the model results allow us to investigate the possible processes of formation and circulation of the intermediate water in the Japan Sea.

4. Formation and circulation of the intermediate water

Using the simulated velocity and hydrographic fields, analysis of the formation and circulation of the intermediate water is attempted through an investigation of subduction processes. Subduction means transfer of the mixed layer water to greater depths and hence it is a key process in the formation and circulation of subsurface water.

a. Method

The subduction process is essentially influenced by the effect of a seasonal cycle of the mixed layer, and is therefore called Stommel's ''mixed-layer demon'' (Marshall et al. 1993; Williams et al. 1995). Water particles detrained from the shallow mixed layer in the summer season are reentrained into the mixed layer as it deepens in the following winter and thus subduction does not occur. In contrast, water particles detrained from the deepest (winter) mixed layer have the possibility of remaining below the mixed layer even after one year, leading to the occurence of substantial subduction. Therefore, the horizontal distribution of the mixed layer when it becomes deepest is a key factor in the subduction process.

To better understand this subduction process in the Japan Sea, it is desirable to investigate the Lagrangian behavior of water movement in detail. For this, we deploy water particles at the time of deepest mixed layer formation and subsequently track them (Fig. 9), using the Euler–Lagrangian technique (Awaji et al. 1991):

$$\frac{d\mathbf{x}}{dt} = \mathbf{u}(\mathbf{x}, t), \tag{12}$$

where $\mathbf{x}$ represents the position of the particle at time t, and $\mathbf{u}$ is the three-dimensional velocity vector. Time integration of (12) is made with a fourth-order Runge–Kutta scheme.

To identify formation areas of the intermediate water, we first calculate the annual mean subduction rate (S_{ann}), defined in the Lagrangian coordinate system (Woods 1985) as

$$S_{\text{ann}}(\mathbf{x}_0) = \underbrace{-\frac{1}{T}\int_0^T w_t(\mathbf{x}_0, t)\, dt}_{\text{vertical displacement}} \underbrace{-\frac{1}{T}\int_0^T \mathbf{u}_t(\mathbf{x}_0, t)\cdot\nabla h(t)\, dt.}_{\text{lateral induction}} \tag{13}$$

The Lagrangian coordinate system is chosen so as to track each water particle at the mixed layer base from the time when it is deepest ($t = 0$), as schematically illustrated in Fig. 9. In the above equation, $\mathbf{x}_0$ represents the horizontal position of a water particle at $t = 0$, $\mathbf{u}_t(\mathbf{x}_0, t)$ and $w_t(\mathbf{x}_0, t)$ are the horizontal and the vertical velocity of a particle, and T is the integration period (1 yr). The first term represents the contribution of vertical displacement of water particles due to Ekman pumping or planetary β effects, and the second term the lateral

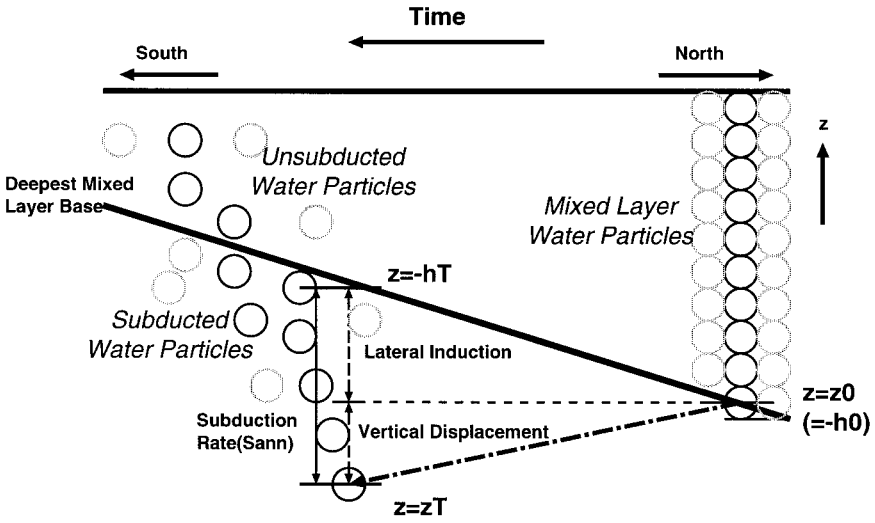

FIG. 9. Schematic picture of the subduction process of the mixed layer water [after Marshall et al. (1993)]. Note that when the subduction rate is estimated, water at any depth is assumed to move with the same horizontal speed as in a Taylor column. In fact, the horizontal velocity with vertical shear transports water particles from one distant region to another and therefore more water is subducted.

induction due to the combined effect of the sloping mixed layer base and the current across it. If each particle trajectory is determined, Eq. (13) can be expressed in a simple form as

$$S_{\text{ann}}(\mathbf{x}_0) = -\frac{1}{T}[z_T - z_0 + h_T - h_0]$$

$$= \frac{1}{T}[-z_T - h_T], \tag{14}$$

where h_0 and h_T are depths of the mixed layer base at $t = 0$ and $t = T$, respectively, and z_0 $(=-h_0)$ and z_T are vertical positions of a water particle at $t = 0$ and $t = T$, respectively. This subduction rate is useful in evaluating the dominant effect on subduction, that is, lateral induction or vertical displacement.

In the estimation of subduction rate, some particles experience abrupt changes of potential density, though deep-water particles, in general, are thought to slowly change potential density as they move. Close examination reveals that these changes are due mainly to the effect of nudging terms. Sparsely distributed nudging terms generate relatively strong local heating/cooling and consequently produce such artificial density changes when particles pass over these grids. For estimates of the subduction rate, therefore, we remove particles with potential density deviations greater than 0.01 σ_θ over a 1-yr travel time, to effectively exclude irregular particles.

Based on particle trajectories over several years, we examine the circulation of the intermediate water in the Japan Sea. We also estimate its formation rate defined as the volume of the mixed layer water detrained into the underlying layer after one year. Qiu and Huang (1995) used the integrated value of the subduction rate over the whole subducted area as the formation rate. Though their study made significant contribution to the understanding of subduction processes, its value gives an approximate estimation because water particles under consideration are assumed to move within a Taylor column (Woods 1985). In the actual oceans, this assumption is not always valid. This is particularly so in regions with a steep slope at the mixed layer base (e.g., a frontal area) where the vertical shear of horizontal velocities is significant due to the thermal wind relation (Fig. 9) and hence the assumption breaks down. In fact, the formation rate estimated by their definition is about two-thirds of our estimation (described later). The influence of the nudging terms on the formation rate will be discussed in section 5.

b. Distribution of the base of the mixed layer

Woods (1985) emphasized a dynamic role of the slope of the mixed layer base such that the lateral induction effectively contributes to the subduction rate as well as the vertical displacement term. Hence, the spatial distribution of the mixed layer base should be determined carefully. In many previous studies, the mixed layer base is defined as the depth at which potential density differs from the surface value by 0.125 σ_θ (Marshall et al. 1993; Qiu and Huang 1995) or 0.05 σ_θ (Williams et al. 1995). However, as discussed by Levitus (1982), such a definition has some problems for our experimental domain, which includes both subtropical and subpolar regions. If density difference is selected for the subtropical (subpolar) region, the mixed layer depth in the subpolar (subtropical) region becomes much shallower (deeper)

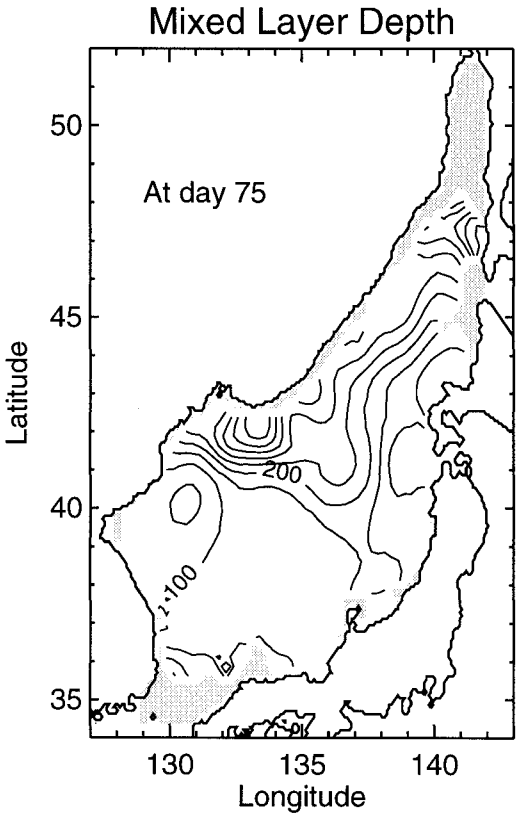

FIG. 10. Distribution of deepest mixed layer base (c.i. = 50 m). The maximum depth is about 500 m near Vladivostok. Large gradients in the mixed layer base can be found near Vladivostok. Shaded areas indicate the occurrence of convection down to the bottom.

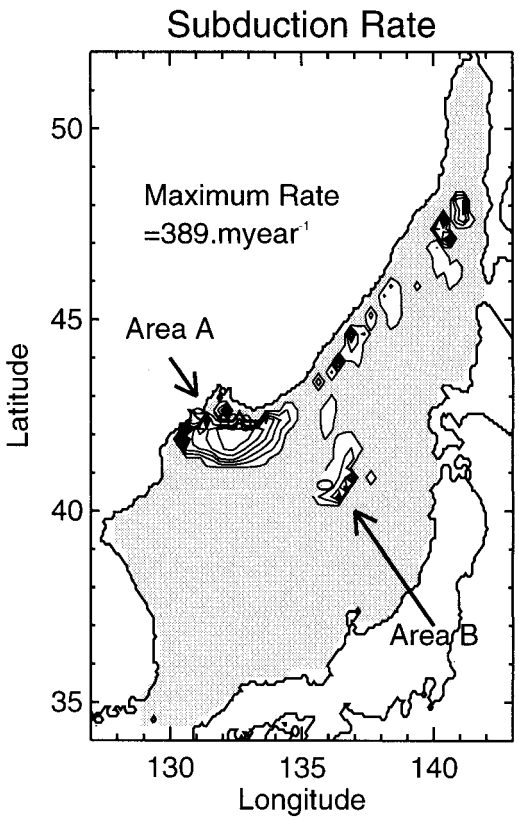

FIG. 11. Distribution of subduction rates (c.i.= 50 m yr^{-1}). Shaded regions indicate the absence of subduction. Local maxima of subduction rates are found in three areas; 41°~43°N west of 135°E (Area A), 40°~43°N east of 136°E (Area B), and north of 45°N.

than is observed, leading to underestimation of the second term on the rhs of (13).

In our model, the convective adjustment operates when unstable stratification is realized. This procedure is a rather simple parameterization for convective mixing. However, the simulated hydrographic field (Fig. 7) captures the basic features of the seasonal cycle of the mixed layer in the Japan Sea, except for a somewhat deeper intermediate layer than is observed, permitting us to define the wintertime mixed layer depth to which convective adjustment operates. This deepest mixed layer develops on about day 75 across the entire basin.

Figure 10 shows the spatial distribution of the deepest mixed layer depth (h_0), demonstrating that the mixed layer is relatively deep along the Primorye coast, with a maximum lying about 500 m off Vladivostok. Seung and Yoon (1995a) reported that the occurrence of intense deep convection down to approximately 1000 m off Vladivostok is limited in severe winters (e.g., 1976/77). However, such relatively deep mixing has been observed only in very severe winters. In fact, the climatological study by Senjyu and Sudo (1996) indicates that the UJSPW formed by deep convection in this area is centered at about 500-m depth. These qualitative features are supported by hydrographic observations made in 1971 (Nitani 1972).

c. Results

A map of subduction rates (S_{ann}) is presented in Fig. 11. Local maxima of subduction rates are found in three areas: 41°~43°N west of 135°E; 40°~43°N east of 136°E; and north of 45°N. The first and second areas are primarily attributed to the lateral induction effect (86%). The third is due mainly to the effect of vertical displacement, but its presence is more uncertain because, as mentioned earlier, the surface potential temperature and salinity used for air–sea fluxes in this area are less reliable. For this reason, our discussion concentrates on the first and second formation areas (henceforth Areas A and B, respectively), though an alongshelf region off Primorye for the third area might be an important source of the deeper water.

Area A, corresponding to the subduction region suggested by Senjyu and Sudo (1993, 1994), has the largest subduction rate (~390 m yr^{-1}). Figure 12 illustrates the initial positions of subducted water particles, and their positions after one, three, and five years. In each panel, the water particle subducted in Area A is represented

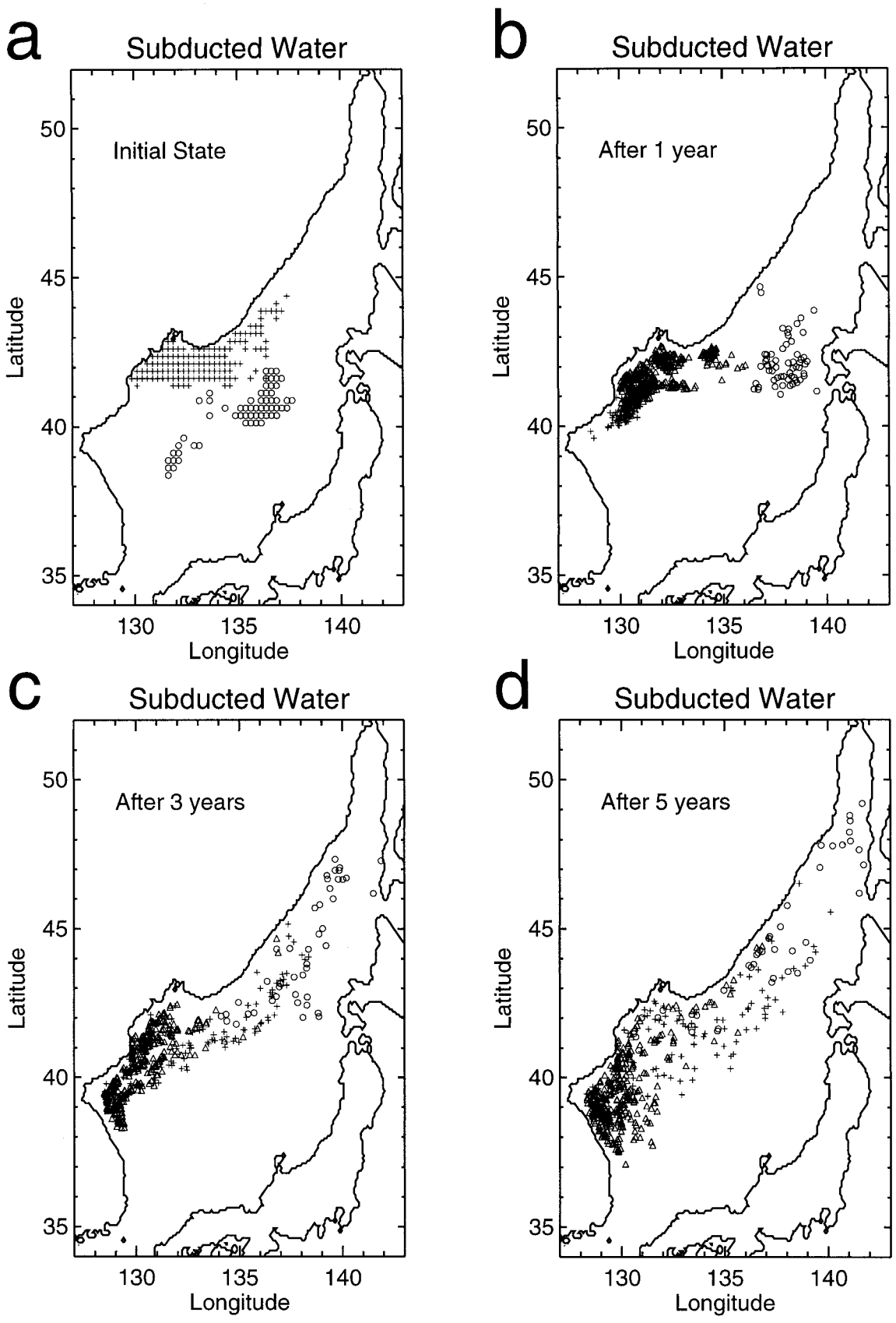
a
Subducted Water
Initial State
b
Subducted Water
After 1 year
c
Subducted Water
After 3 years
d
Subducted Water
After 5 years
Latitude
Longitude
50
45
40
35
130
135
140

by a plus sign if its depth is shallower than 200-m depth and a triangle if greater than 200 m, while the water particle in Area B is denoted by a circle sign. (Note that only in Fig. 12a, all particles subducted in Area A are represented by plus signs for clarification.) From Figs. 12a and 12b, mixed layer particles in Area A are transported southwestward into subsurface regions where the overlying mixed layer is much shallower due to the presence of considerably strong western/coastal boundary currents along the continent (Fig. 5c). This causes the most effective subduction of the mixed layer water into the intermediate layer in the Japan Sea. Thus, the vertical displacement effect on subduction of the intermediate water is small in the Japan Sea. Note that the North Pacific Intermediate Water moves southward to interior regions, whereas in the Japan Sea newly formed intermediate water advects to the south along the western boundary region because of positive wind stress curl in winter over almost the whole of the Japan Sea.

After arriving at about 39°N, most particles shallower than 200-m depth (e.g., relatively low salinity water along the continent) deflect northeastward along the subpolar front to reach the eastern part of the Japan Basin (Figs. 12c,d). On the other hand, deeper particles (below 200 m) flow farther southward in the intermediate layer along the Korean coast. To see the behavior in more detail, the pathways and salinity histories of two typical deeper particles are shown in Fig. 13. The lighter one ($<32.00\ \sigma_1$) is denoted by a solid line and the heavier one (categorized as the UJSPW) by a broken line. This figure demonstrates that the lighter particle moves southward and reaches about 37°N in 6~7 years, forming the simulated SML (less than 34.06 psu as shown in Fig. 13b). Afterward, it moves westward to the EKWC and then to the northeast. This particle movement indicates that the SML is composed of subducted water in Area A.

However, the observed SML water off the Korean coast (i.e., ESIW) extends to the south around 35.5°N (Kim and Chung 1984). In our model, the water particle does not reach such a southern location. Thus, the ESIW south of 37°N is not reproduced. This is attributed to the formation of a warm eddy centered at a location (38.5°N, 130°E) in August (Fig. 6c), which is associated with an overshooting of the EKWC. Insufficient representation of this eddy in the model prevents transport of the lighter particles farther southward (Fig. 13a). In contrast, the heavier particle below this eddy can proceed farther south.

Though some model results are not in quantitatively good agreement with the observations, the above consideration anticipates that the ESIW observed near the Korean coast (Kim and Chung 1984) is the intermediate water subducted in Area A, and hence the origins and transport processes of the ESIW and the UJSPW are basically similar. The differences in their locations and properties arise from the fact that the ESIW is formed by shallow convection on the southern side of Area A, whereas the UJSPW is formed by deeper convection on the northern side down to the depth where salinity is relatively high (Fig. 14). In addition, faster advection of the ESIW relative to the UJSPW makes it fresher and higher dissolved-oxygen concentration in the Tsushima Basin. Taking into consideration these facts, the ESIW and the UJSPW can be referred to as the upper portion and the lower portion of the Japan Sea intermediate water (schematically shown in Fig. 15).

The formation of intermediate water in Area B has never been reported to date. Water subducted there (indicated by circle signs in Fig. 12a) is advected northeastward and then northward into the subsurface layer between the Tsugaru Warm Current and 300-m depth off Hokkaido (Fig. 12b). The presence of this transport is corroborated by a local maximum in the dissolved oxygen content extending from the surface to the corresponding depth in that region (Fig. 16). After transport farther northward for several years, some of this subducted water flows out through Soya Strait or is reentrained into the mixed layer off the Primorye coast. The subduction rate in Area B amounts to about 150 m yr^{-1} at its maximum.

Overall features of the basin-scale circulation of the intermediate water are studied using the annual mean Lagrangian velocities on the 32.00 σ_1 surface (Fig. 17) corresponding to the top of the UJSPW. Note that seasonal variation in velocities in the intermediate layer is significant (Figs. 5 and 6) and hence the calculated mean Lagrangian velocity field is considerably different from that obtained by steady-state models. In Fig. 17, southward transport of the intermediate water takes two major routes: along the continent in winter (Fig. 5c) and along the Japanese coast in summer (Fig. 6c). Senjyu and Sudo (1996) suggested that the UJSPW is transported eastward into the Yamato Basin with a travel time of 12~15 months. However, such transport is not seen in the mean velocity field. One reason for this deficiency is the rough resolution of the geometry of the YR. Actually, the YR is a very high seamount, the top of which is situated only about 300 m below sea surface and hence an anticyclonic flow, the so-called Taylor cap, could be dominant near the peak (Chapman and Haidvogel 1991). This anticyclonic flow may transport some of the

←

FIG. 12. Positions of subducted water particles launched at day 75: (a) initial position, (b) after 1 yr, (c) after 3 yr, and (d) after 5 yr. The water particle subducted in Area A is represented by a plus sign if its depth is shallower than 200-m depth and a triangle if greater than 200 m, while the water particle in Area B is denoted by a circle sign. In (a) all particles subducted in Area A are represented by plus signs for clarification.

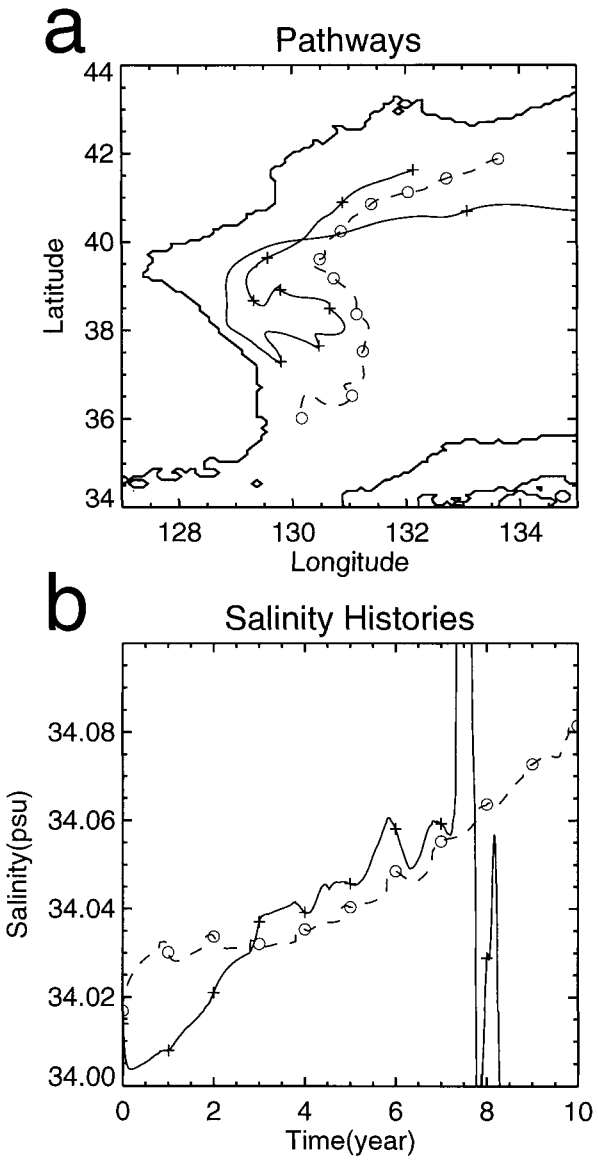

FIG. 13. The (a) pathways and (b) salinity histories of the two typical deeper (>200 m) particles subducted in Area A. The solid line indicates the lighter (<32.00 σ_1) particle (corresponding to the ESIW) and the broken line indicates the heavier (>32.00 σ_1) one (corresponding to the UJSPW). Plus and circle signs are marked every year. Marked salinity fluctuation of the lighter particle [solid line in panel (b)] after 7 yr is due to significant seasonal variation after its surfacing.

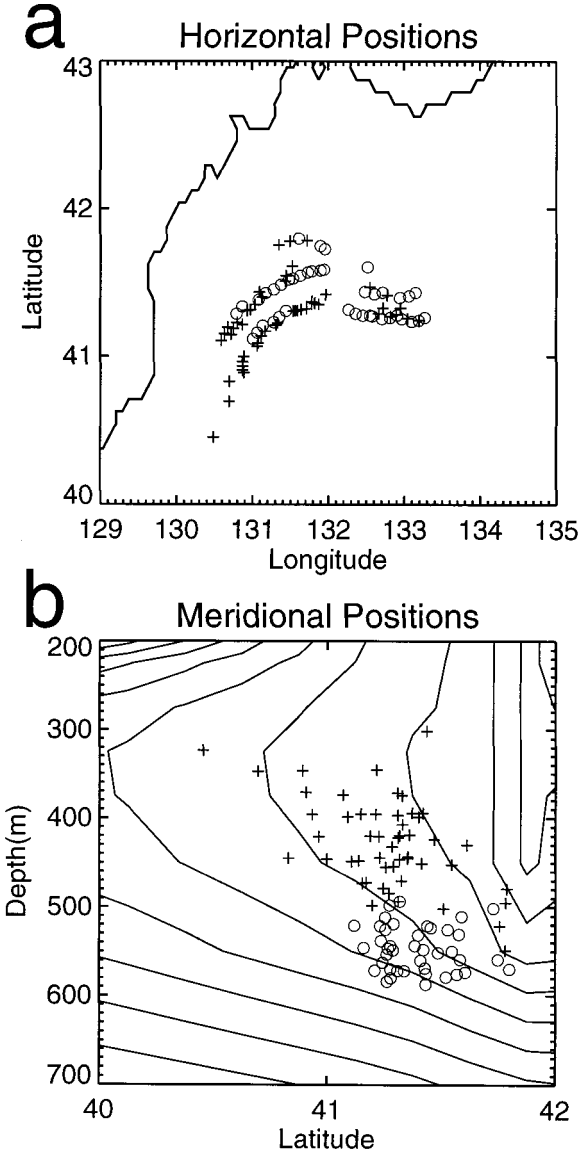

FIG. 14. The (a) horizontal and (b) meridional particle positions of the ESIW (plus sign) and UJSPW (circle sign) after 1 yr. Contour lines in panel (b) represent salinity distribution along about 132°E (c.i. = 0.01 psu).

UJSPW into the Yamato Basin by way of the YR. Another reason is an artificial intensification of upwelling along the eastern coast of Korea due to the "Veronis effect" (basically arising from neglect of isopycnal mixing processes) (e.g., Veronis 1975; Hirst and McDougall 1996). In the absence of this artificial upwelling, therefore, the significant basin-scale anticyclonic circulation in winter described earlier could transport the intermediate water into the ocean interior (Seung 1997), followed by southward advection into the Yamato Basin due to the significant southward undercurrent beneath the NB in the summer season.

Figure 18 shows a diagram of formation rates for each potential density surface (σ_1). The mixed layer water in the Japan Sea is subducted mainly onto density surfaces ranging from 31.70 to 32.03 σ_1, with the largest portion (57.7%) being on the 31.95~32.00 σ_1 surface. The total formation rate amounts to 0.48 Sv, 87.5% (0.42 Sv) of which takes place in Area A.

Senjyu and Sudo (1996) estimated a formation rate for the UJSPW to be 0.48 Sv between the 32.00 and 32.05 σ_1 surfaces, whereas the value estimated in this study is only 0.06 Sv. Our small formation rate is at-

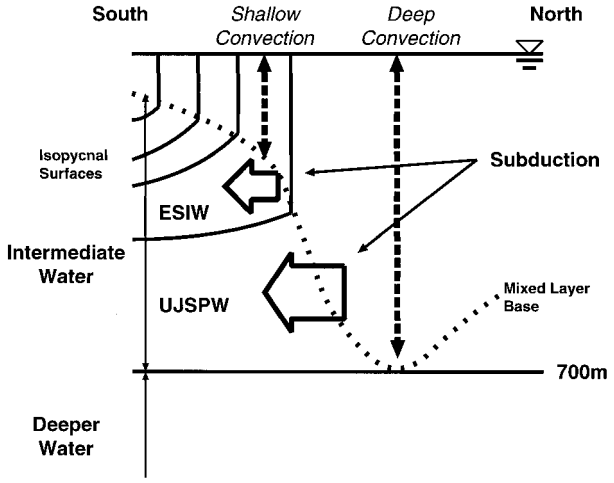

FIG. 15. Schematic picture of the subduction process of the ESIW and the UJSPW.

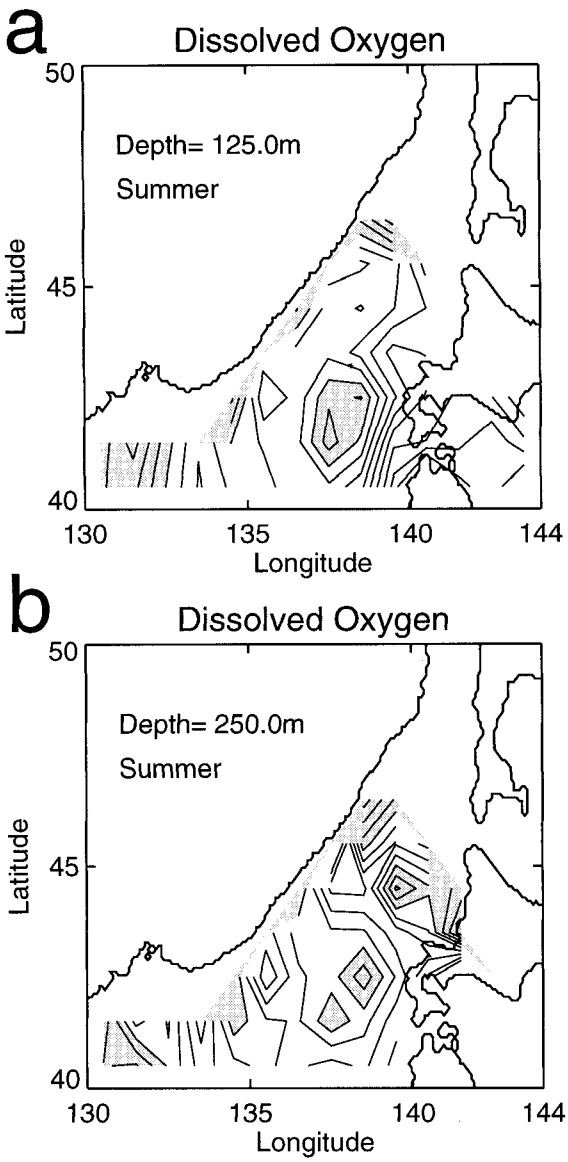

FIG. 16. Horizontal distribution of dissolved oxygen content in the summer season (a) at 125-m and (b) 250-m depth. Contour intervals are 0.1 ml l^{-1}. Shaded areas indicate dissolved oxygen content higher than 6.8 ml l^{-1} for (a) and 6.5 ml l^{-1} for (b), respectively. These values are estimated by averaging the observational data (NODC) onto $1° \times 1°$ grids. The values along the continental coast and in the northernmost area are missing (no observations).

tributed partly to weak surface cooling in winter described before. In fact, water denser than 32.03 σ_1 is not formed in our model. Another reason for this discrepancy is whether or not a reentrainment process into the mixed layer with seasonal variation is taken into account. In estimating the formation rate of the UJSPW, Senjyu and Sudo assumed a steady-state ventilation process in which all the outcropping water in winter (corresponding to the mixed layer water in Fig. 9) was subducted into the intermediate layer and never returned. However, as pointed out by previous studies on Stommel's mixed layer demon (e.g., Williams et al. 1995; Qiu and Huang 1995), subduction processes are greatly influenced by seasonal change in the mixed layer. Hence, some outcropping water in winter is most likely reentrained into the mixed layer until the following winter. In fact, our detailed analysis of the model results within a seasonal forcing scenario demonstrates that a portion of the outcropping water, which amounts to 0.13 Sv if it is subducted, remains at relatively shallow depth. Here, its potential density evolves in subsequent seasons and it is reentrained into the mixed layer in the next winter, thus reducing the formation rate. This means that the effect of seasonal variations on the subduction process should be taken into account for better estimation.

When the intermediate water in the Japan Sea is defined as the water between 31.65 and 32.03 σ_1 surfaces, the total volume of the intermediate water is 3.88×10^{14} m^3 and the ventilation time is estimated to be 25.6 yr using the formation rate obtained here. This ventilation time is much shorter than that for the deep circulation, about 100~300 yr, as estimated by several chemical tracer studies (e.g., Chen and Wang 1995). This suggests that the intermediate circulation is indicative of decadal variabilities in the Japan Sea. This remains a subject for future study.

5. Discussion

As discussed by Toggweiler et al. (1989), the nudging term in robust diagnostic models has a tendency to suppress vertical velocity relative to results from prognostic models through creation of denser water in deep layers. On this point, we examined what effect the nudging term has on the formation of intermediate water in our model. Hence, we ran both a prognostic model (henceforth called PROGM) and a robust diagnostic model (henceforth DIAGM) in addition to the nudging model

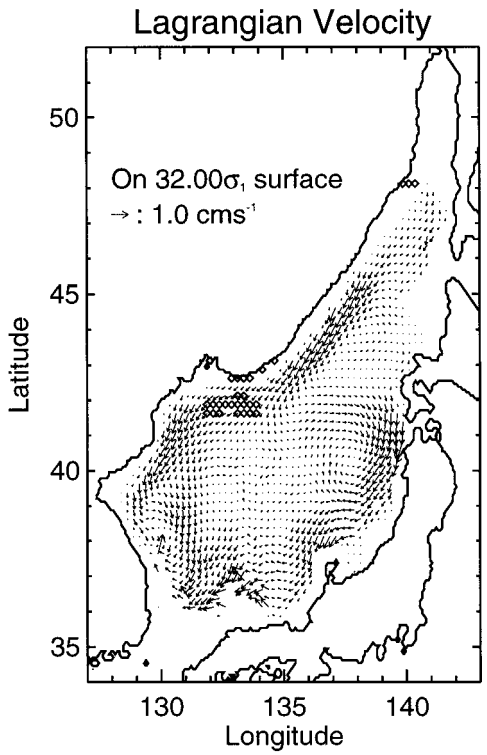

FIG. 17. Annual mean Lagrangian velocity of the particles launched on a 32.00 σ_1 surface at day 75. This surface corresponds to the top of the UJSPW. Regions with a diamond mark represent outcropping areas.

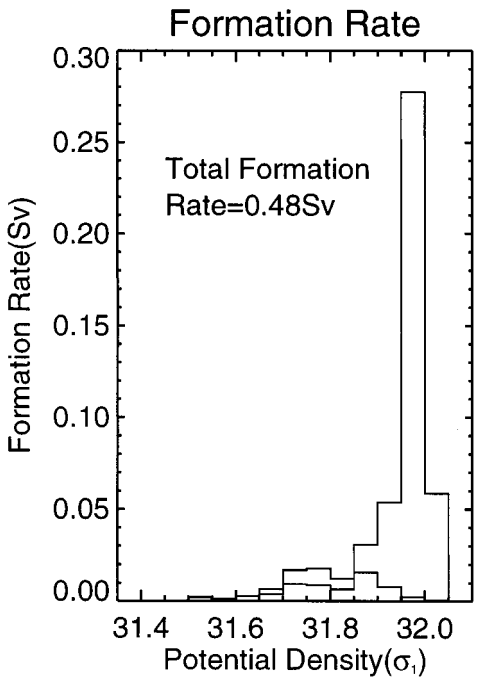

FIG. 18. Formation rate as a function of potential density. The lower line indicates the formation rate in Area B.

(henceforth NUDGM). In PROGM, there is no nudging term except within the top level at which thermohaline forcing is imposed. In contrast, DIAGM retains the nudging effect on θ and S for all boxes. Here the results obtained by NUDGM are used temporarily to generate θ^* and S^* required in DIAGM except that both calculated potential temperature and salinity below 600 m are lowered by about 0.4°C and 0.1 psu to better reproduce observed hydrographic features in the deeper layer. These two additional experiments are conducted under the same conditions as in NUDGM, and then the formation and circulation of the intermediate water are examined as before.

We found that there is no significant difference in the formation areas of the intermediate water among these three experiments (Figs. 11 and 19). This is primarily due to the fact that the formation areas are determined mainly by horizontal structure in the mixed layer depth, which, as a result of the same air–sea flux condition, is similar in each experiment.

The major circulation features of the intermediate water also are basically similar among these three experiments (not shown). For example, the annual mean Lagrangian velocity on the 32.00 σ_1 surface in both PROGM and DIAGM results shows southward transport of intermediate water along two routes similar to those in NUDGM, though minor differences can be seen.

In contrast, the formation rate seems sensitive to the restoring forcing. The formation rate and the ventilation time in these three experiments are listed in Table 2. The formation rate using PROGM is largest (0.69 Sv). This is caused by more active deepening of the mixed layer near formation areas (maximum depth of about 640 m) in PROGM in association with the presence of the lighter intermediate layer than in the other two models, as discussed below. It is easily understood from Fig. 9 that, if the mixed layer becomes deeper near the formation areas, the formation rate becomes larger due to the enhancement of the effect of lateral induction. This is marked in Area B. For example, some of the subducted water particles from Area B are effectively captured by the intense undercurrent beneath the NB and transported directly into the Yamato Basin. On the other hand, the formation rate from DIAGM is almost the same as that from NUDGM (0.53 Sv), suggesting that the restoring force in the deeper layer does not affect intermediate water formation rates significantly.

As discussed by Sarmiento and Bryan (1982) and Miyama et al. (1995), both DIAGM and NUDGM are less sensitive to the choice of eddy diffusivity than is PROGM because of the presence of the restoring terms. Associated with this, the effect of vertical diffusion on the PROGM-induced pycnocline in the subtropical region (above about 300-m depth) is to make it deeper and to deflect it more northward in comparison with the other two models, as found by Seung and Kim (1993). This also means lighter intermediate water for the case of PROGM (Fig. 20a). Such modification of a pycno-

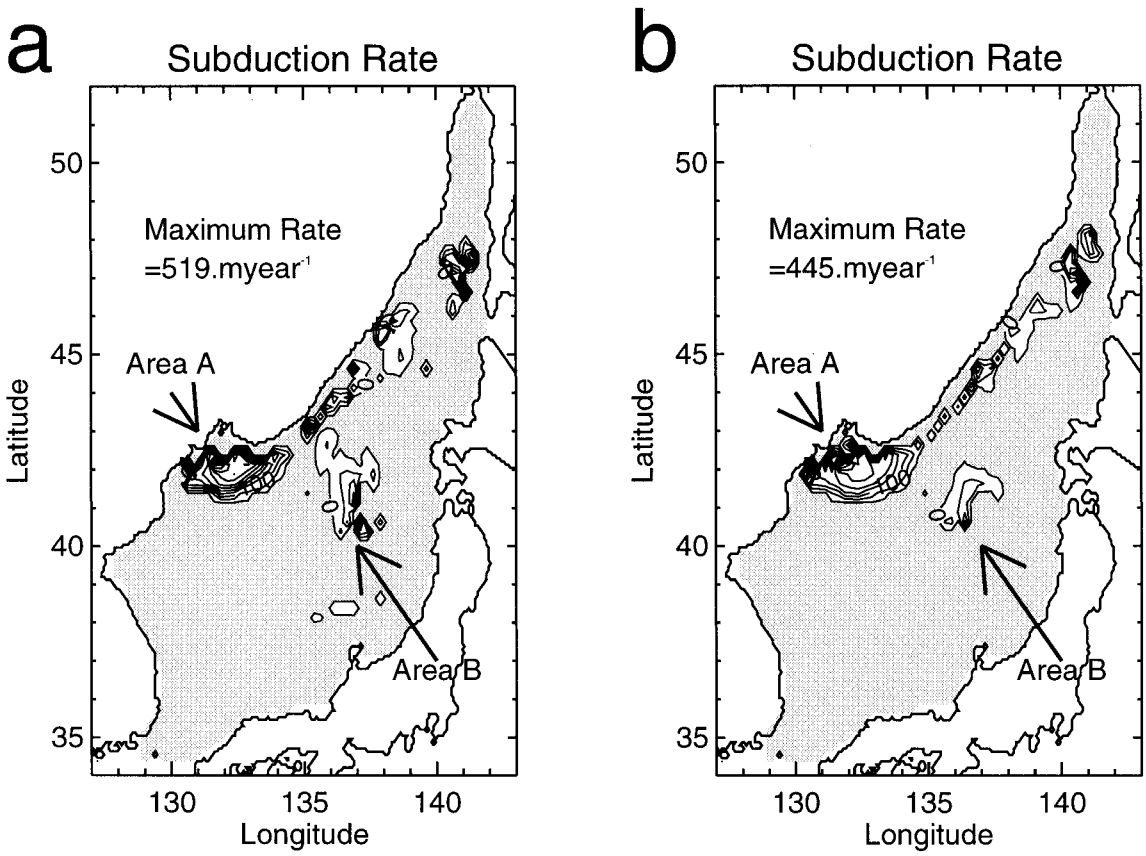

FIG. 19. Same as Fig. 11 but for (a) PROGM and (b) DIAGM.

cline pattern in the subtropical region enables far northward continuation of the EKWC through the thermal wind relation, leading to an overshooting of this current (Fig. 21). In NUDGM, on the other hand, the nudging effect acts to keep a shallow pycnocline (Fig. 20b), and thus the overshooting of the EKWC is largely suppressed. However, as mentioned earlier, since the effect of baroclinic instability is not fully represented, the pycnocline is still deeper than is observed. In addition, recent observational and theoretical studies reported that the baroclinic instability plays an important role on the breaking and spreading of deep water formation (e.g., Jones and Marshall 1993). Improvement of our model will be required to fully resolve this effect and this is currently under way.

Finally, gross water-mass transport along a meridian is discussed by calculating the meridional streamfunction in February (Fig. 22a) and August (Fig. 22b). This is obtained by a longitudinal integration of the north/southward velocity component (v) from bottom to surface (water moves in the sense such that large streamfunction values are on the right). Note that all of the contours do not close due to the presence of in/outflow through the straits. The patterns obtained with NUDGM (Fig. 22) are qualitatively similar to those with PROGM and DIAGM. In Fig. 22, large amounts of intermediate water are transported southward in both months. There seems to be two cells in February—an upper one located between 200 m and 400 m and a lower one below about 400 m. The lower cell is present from November to March. A close look at Fig. 22 indicates that intense southward transport of the intermediate water along the continent in wintertime is compensated partly by upwelling of the deeper water. On the other hand, southward transport of the intermediate water along the Japanese coast in summertime is likely to be compensated by surface water. This seasonal reversal of circulation below 1000 m seems curious, because in winter, it contains a upwelling of the deeper water in the Cold Current Region and a downwelling in the Warm Current Region in the opposite sense to the buoyancy forcing. This overturning in the model is driven by the strong wind stress of the winter monsoon. In the northern half region, large

TABLE 2. Formation rate and ventilation time in each experiment.

		NUDGM	DIAGM	PROGM
Formation rate (Sv)	Total	0.48	0.53	0.69
	Area A	0.42	0.44	0.44
	Area B	0.06	0.09	0.25
Volume ($\times 10^{14}$ m^3)		3.88	3.38	5.22
Ventilation time (yr)		25.6	20.3	23.8

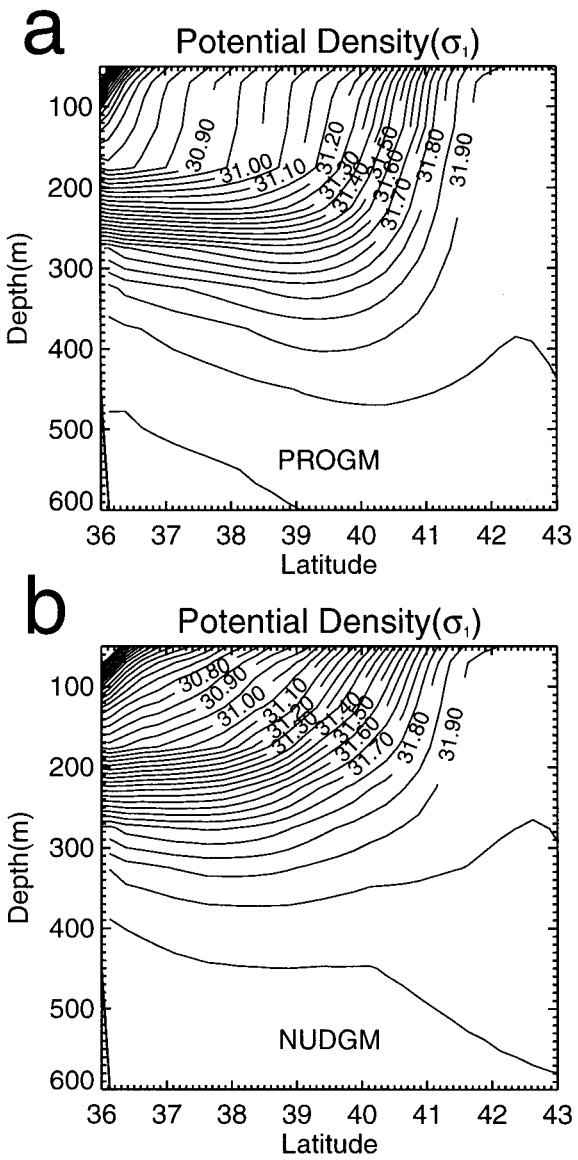

FIG. 20. Meridional distribution of potential density along 131.12°E in (a) PROGM and (b) NUDGM for Aug.

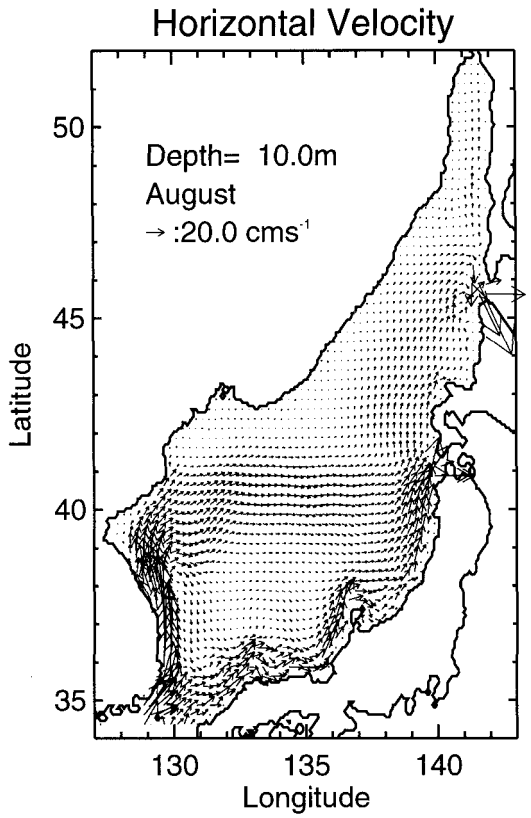

FIG. 21. As in Fig. 6b but for PROGM.

negative wind stress curl generates a strong Ekman upwelling, and this effect can penetrate into deep layers due to weak stratification. Although a similar phenomenon has been discussed in an Antarctic context by Toggweiler (1994), the thermohaline forcing in our model may be weaker than exists in reality. Hence it should be confirmed by future observations whether or not this seasonal reversal of deep circulation is realized in practice. Our results show that the effect of strong wind stress in winter has the ability to cause the seasonal reversal of the deep cell in opposition to buoyancy forcing. Considering the recent report of Riser (1997), which gave historical evidence for a lack of formation of the deeper water since the 1970s, the reversal has probably taken place in recent relatively warm phases.

6. Summary

Using a nudging model, the formation and circulation of the intermediate water in the Japan Sea have been investigated by study of subduction processes of the mixed layer water. Though the nudging term was taken into account in the relatively small number of grid boxes compared with a full robust diagnostic model, the simulated seasonal variation of velocity and hydrographic fields were in qualitatively good agreement with observations.

Two major formation areas of the intermediate water were identified. Area A (41°~43°N, west of 135°E) corresponds to the subduction region suggested by Senjyu and Sudo (1993, 1994). Area B (40°~43°N, east of 136°E) has never been reported so far but is supported by observations of dissolved oxygen concentration. The subducted water from the mixed layer in Area A is advected southwestward by intense western/coastal boundary currents along the continent. Later, a shallower portion (above 200 m) deflects northeastward along the subpolar front, whereas a deeper branch (below 200 m) continues southward into the Tsushima Basin over a travel time of 6~7 years, forming the ESIW. This fact suggests that both the ESIW and the UJSPW have the same origin, that is, the mixed layer water in Area A in the Cold Current Region. In addition, the processes transporting them from the formation area are physically

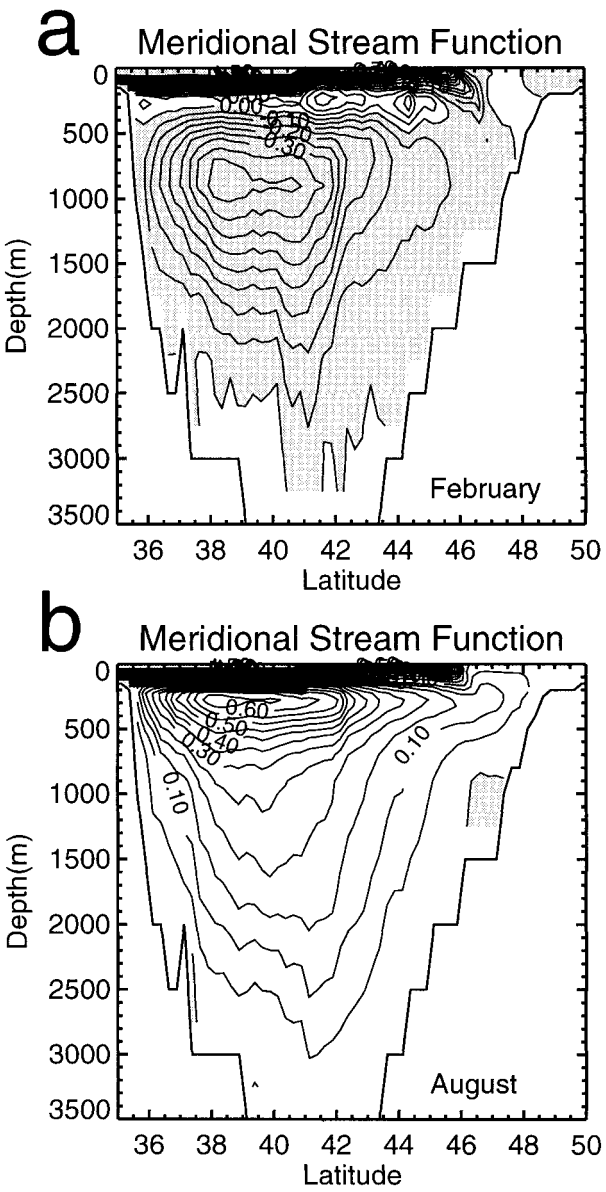

FIG. 22. Meridional streamfunction for (a) Feb and (b) Aug in NUDGM. Shaded areas represent negative values.

identical. Differences in their locations and properties arise from the fact that the ESIW is formed by shallow convection on the southern side of Area A, whereas the UJSPW is formed by deeper convection down to 500 m on the northern side. Therefore, the ESIW and the UJSPW can be thought to correspond to the upper and lower portions of the intermediate water, respectively.

The subducted water from Area B is directed into the eastern part of the Japan Basin, and some of it flows out to the North Pacific through the Soya Strait and/or returns into the mixed layer off the Primorye coast. The subduction in these two areas is attributed mainly to the effect of lateral induction.

Detailed circulation processes of the UJSPW are examined by tracking water particles on a 32.00 σ_1 surface, revealing that its southward transport takes two major routes: along the continent in wintertime and along the Japanese coast in summertime. The estimated total formation rate of the intermediate water ranges from 0.48 to 0.69 Sv according to the strength of the nudging term. Our analysis reveals that the effect of seasonal variations of mixed layer processes should be taken into account. The ventilation time is estimated to be 20.3~25.6 yr, which is shorter than the timescale for the basin-scale deep circulation (about 100~300 yr) suggested by previous chemical tracer observations.

In this study, climatological features of the formation and circulation of the intermediate water were investigated. Using the existing hydrographic data and the numerical models, possible processes for the formation and circulation of the intermediate water were proposed. However, due partly to the limits of the current OGCM and partly to the limits imposed by the paucity of observations, studies of this type of problem are challenging and several issues remain to be resolved. The most important one concerns the parameterization for deep convection. In this study, a simple parameterization (i.e., conventional convective adjustment) was used, but this is insufficient for further detailed analysis. In future, direct treatment for convective mixing processes (such as using 3D nonhydrostatic models) will be required. More accurate air–sea heat and salt fluxes, particularly in the northern region, and precise resolution of the effect played by baroclinic instability are also important to realize better understanding of the formation and circulation processes. Thus, for a complete identification and characterization of the processes involved in the deep water formation and its circulation in the Japan Sea, further observation and modeling are required.

Acknowledgments. We express our hearty thanks to Dr. J. P. Matthews for his critical reading. Part of this study was supported by a Grant-in-Aid for Scientific Research, number 3265, from the Ministry of Education, Science, Culture, Japan. The numerical calculation was carried out on FACOM M1800 and VP2600 at the Data Processing Center of Kyoto University.

REFERENCES

Aota, M., and M. Ishikawa, 1991: Fresh water supply to the sea of Okhotsk and volume transport of Soya Warm Current (in Japanese with English abstract). *Bull. Hokkaido Nat. Fish. Res. Inst.,* **55,** 95–99.

Armi, L., and N. A. Bray, 1982: A standard analytic curve of potential temperature versus salinity for the western North Atlantic. *J. Phys. Oceanogr.,* **12,** 384–387.

Awaji, T., 1982: Water mixing in a tidal current and the effect of turbulence on tidal exchange through a strait. *J. Phys. Oceanogr.,* **12,** 501–514.

——, K. Akitomo, and N. Imasato, 1991: Numerical study of shelf water motion driven by the Kuroshio: Barotropic model. *J. Phys. Oceanogr.,* **21,** 11–27.

Bryan, K., and M. D. Cox, 1972: An approximate equation of state for numerical models of ocean circulation. *J. Phys. Oceanogr.*, **2,** 2510–2514.

Chapman, D. C., and D. B. Haidvogel, 1991: Formation of Taylor caps over tall isolated seamount in a stratified ocean. *Geophys. Astrophys. Fluid Dyn.,* **64,** 31–65.

Chen, C. T. A., and S. L. Wang, 1995: Carbonate chemistry of the sea of Japan. *J. Geophys. Res.,* **100,** 13 737–13 745.

Ghil, M., and P. Malanotte-Rizzoli, 1991: Data assimilation in meteorology and oceanography. *Advances in Geophysics,* Vol. 33, R. Dmowska and B. Saltzman, Eds., Academic Press, 141–266.

Haines, K., P. Malanotte-Rizzoli, R. E. Young, and W. R. Holland, 1993: A comparison of two methods for assimilation of altimeter data into a shallow-water model. *Dyn. Atmos. Oceans,* **17,** 89–133.

Haney, R. L., 1971: Surface boundary condition for ocean circulation models. *J. Phys. Oceanogr.,* **1,** 241–248.

Hase, H., J. H. Yoon, and M. Takematu, 1997: The current structure of the Tsushima Current over the shelf off the Wakasa Bay during 1995–96. *Proc. Second CREAMS'97 Int. Symp.,* Fukuoka, Japan, Res. Inst. App. Mech., Kyushu University, 71–74.

Hirose, N., C. H. Kim, and J. H. Yoon, 1996: Heat budget in the Japan Sea. *J. Oceanogr. Soc. Japan,* **52,** 553–574.

Hirst, A. C., and T. J. McDougall, 1996: Deep-water properties and surface buoyancy flux as simulated by a *Z*-coordinate model including eddy-induced advection. *J. Phys. Oceanogr.,* **26,** 1320–1343.

Holloway, G., T. Sou, and M. Eby, 1995: Dynamics of circulation of the Japan Sea. *J. Mar. Res.,* **53,** 539–569.

Isoda, Y., and M. Nishihara, 1992: Behavior of warm eddies in the Japan Sea (in Japanese with English abstract). *Umi to Sora,* **67,** 53–65.

Japan Oceanographic Data Center, 1978: *Marine Environmental Atlas, Northwestern Pacific Ocean II (Seasonal–Monthly).* Japan Hydrographic Association, 157pp.

Jones, H., and J. Marshall, 1993: Convection with rotation in a neutral ocean: A study of open-ocean deep convection. *J. Phys. Oceanogr.,* **23,** 1009–1039.

Katoh, O., 1993: Detailed current structures in the eastern channel of the Tsushima Strait in summer. *J. Oceanogr. Soc. Japan,* **49,** 17–30.

——, 1994: Structure of the Tsushima Current in the southwestern Japan Sea. *J. Oceanogr. Soc. Japan,* **50,** 317–338.

Kim, K., and J. Y. Chung, 1984: On the salinity-minimum and dissolved oxygen-maximum layer in the East Sea (Sea of Japan). *Ocean Hydrodynamics of the Japan and East China Seas,* T. Ichiye, Ed., Elsevier, 56–66.

Kitani, K., 1987: Direct current measurement of Japan Sea Proper Water (in Japanese). *Nihon. Suis. Shik. Kenky. Renr. News,* **341,** 1–6.

Levitus, S., 1982: *Climatological Atlas of the World Ocean.* National Oceanic and Atmospheric Administration, 173 pp.

Lie, H. J., M. S. Suk, and C. H. Kim, 1989: Observations of southeastward deep currents off the east coast of Korea. *J. Oceanol. Soc. Korea,* **24,** 63–68.

Marshall, J. C., A. J. G. Nurser, and R. G. Williams, 1993: Inferring the subduction rate and period over the North Atlantic. *J. Phys. Oceanogr.,* **23,** 1315–1329.

Minato, S., and R. Kimura, 1980: Volume transport of the western boundary current penetrating into a marginal sea. *J. Oceanogr. Soc. Japan,* **36,** 185–195.

Miyama, T., T. Awaji, and K. Akitomo, 1995: Study of seasonal transport variations in the Indonesian Sea. *J. Geophys. Res.,* **100,** 20 517–20 541.

Moriyasu, S., 1972: The Tsushima Current. *Kuroshio,* H. Stommel and K. Yoshida, Eds., University of Washington Press, 352–369.

Na, J. Y., J. W. Seo, and S. K. Han, 1992: Monthly-mean sea surface winds over the adjacent seas of the Korean Peninsula. *J. Oceanol. Soc. Korea,* **27,** 1–10.

Nitani, H., 1972: On the deep and the bottom waters in the Japan Sea. *Researches in Hydrography and Oceanography,* D. Shouji, Ed., Hydrographical Department of Japan Maritime Safety Agency, 151–201.

Ohshima, K., 1994: The flow system in the Japan Sea caused by a sea level difference through shallow straits. *J. Geophys. Res.,* **99,** 9925–9940.

Qiu, B., and R. X. Huang, 1995: Ventilation of the North Atlantic and North Pacific: Subduction versus obduction. *J. Phys. Oceanogr.,* **25,** 2374–2390.

Redfield, A. C., B. H. Ketchum, and F. A. Richards, 1963: The influence of organisms on the composition of seawater. *The Sea,* Vol. 2, M. N. Hill, Ed., Interscience, 26–77.

Riser, S. C., 1997: Long-term variations in deep ventilation of the Japan/East Sea. *Proc. Second CREAMS'97 Int. Symp.,* Fukuoka, Japan, Res. Inst. App. Mech., Kyushu University, 31–34.

Sarmiento, J. L., and K. Bryan, 1982: An ocean transport model for the North Atlantic. *J. Geophys. Res.,* **87,** 394–408.

Senjyu, T., and H. Sudo, 1993: Water characteristics and circulation of the upper portion of the Japan Sea Proper Water. *J. Mar. Sys.,* **4,** 349–362.

——, and ——, 1994: The upper portion of Japan Sea Proper Water. Its source and circulation as deduced from isopycnal analysis. *J. Oceanogr. Soc. Japan,* **50,** 663–690.

——, and ——, 1996: Interannual variation of the upper portion of the Japan Sea Proper Water and its probable cause. *J. Oceanogr. Soc. Japan,* **52,** 27–42.

Seung, Y. H., 1997: Ventilation of intermediate water in the East Sea. *Proc. Second CREAMS'97 Int. Symp.,* Fukuoka, Japan, Res. Inst. App. Mech., Kyushu University, 7–10.

——, and K. Kim, 1989: On the possible role of local thermal forcing on the Japan Sea Circulation. *J. Oceanol. Soc. Korea,* **24,** 29–38.

——, and ——, 1993: A numerical modeling of East Sea Circulation. *J. Oceanol. Soc. Korea,* **28,** 292–304.

——, and J. H. Yoon, 1995a: Some features of winter convection in the Japan Sea. *J. Oceanogr. Soc. Jpn.,* **51,** 61–73.

——, and ——, 1995b: Robust diagnostic modeling of the Japan Sea circulation. *J. Oceanogr. Soc. Jpn.,* **51,** 421–440.

Shikama, N., 1994: Current measurements in the Tsugaru Strait using bottom-mounted ADCPs (in Japanese). *Kaiyo Mon.,* **26,** 815–818.

Sudo, H., 1986: A note on the Japan Sea Proper Water. *Progress in Oceanography,* Vol. 17, Pergamon, 313–336.

Toggweiler, J. R., 1994: The ocean's overturning circulation. *Physics Today,* **47,** 45–50.

——, K. Dixon, and K. Bryan, 1989: Simulations of radiocarbon in a coarse-resolution World Ocean model 1. Steady state prebomb distribution. *J. Geophys. Res.,* **94,** 8217–8242.

Uda, M., 1934: The results of simultaneous oceanographical investigations in the Japan Sea and its adjacent waters in May and June (in Japanese). *J. Imp. Fish. Exp. Sta.,* **5,** 57–190.

UNESCO, 1978: Eighth report of the Joint Panel on Oceanographic Tables and Standards. *UNESCO Tech. Rep. Mar. Sci.,* **28,** 35 pp.

Veronis, G., 1975: The role of models in tracer studies. *Numerical Models of the Ocean Circulation.* Natl. Acad. Sci., 133–146.

Williams, R. G., M. A. Spall, and J. C. Marshall, 1995: Does Stommel's mixed-layer ''demon'' work? *J. Phys. Oceanogr.,* **25,** 3089–3102.

Woods, J. D., 1985: The physics of thermocline ventilation. *Coupled Ocean–Atmosphere Models,* J. C. J. Nihoul, Ed., Elsevier, 543–590.

Yasui, M., T. Yasuoka, and O. Shiota, 1967: Oceanographic studies of the Japan Sea. Part I: Water characteristics. *Oceanogr. Mag.,* **19,** 177–192.

Yoon, J. H., 1982: Experiment on the circulation in the Japan Sea. Part I. Formation of the East Korean Warm Current. *J. Oceanogr. Soc. Japan,* **38,** 43–51.

——, and N. Hirose, 1995: The barotropic response to the wind in the Japan Sea. *Extended Abstracts, First Int. Marine Science Symp.,* Matsue, Japan, Japan Marine Science Foundation, 38–39.